Chapter IV

Nickel (II)-pterin coordination chemistry in presence of 1, 2-diaminoethane as the ancillary ligand: synthesis, structural and comparative reactivity studies for aqua and imidazole substituted complexes in the light of DFT

Abstract

A 6-substituted pterin ligand 7-methylpterin-6-carboxylic acid (H_2L) plays a pivotal role for the present study; it is complemented by a typical ligand like σ- donor ancillary ligand like 1,2-diaminoethane(en). Solubility of H_2L in aqueous alkali permits the synthesis of a mononuclear nickel(II) complex $[Ni^{II}(L)(en)(H_2O)]. 2H_2O$ (**1**) from this medium in the crystalline form and its x-ray structural characterization. Again, the use of imidazole (Im) as an additional supporting ligand, permits the synthesis and x-ray structural characterization of another new complex $[Ni(L)(en)(Im)]. 2H_2O$ (**2**). Their microanalytical, spectroscopic, magnetic susceptibility, cyclic voltammetric and reactivity data are quite valuable for characterization purpose. Both of them are chiral; their longer wavelength (755 -769 nm) positive cotton effect may be correlated with the δ-conformation of the 'en' chelate ring. Reactivity of **1** towards imidazole (Im) is characterized by substrate saturation kinetics as well as a negative $\Delta S^{\neq}$ value (-178.5 J mol^{-1} deg^{-1}), indicating an associative pathway. The μ_{eff} values (BM) are consistent with the presence of Ni(II) centres in these complexes, while cyclic voltammetric data point towards a metal-centred [Ni(II) → Ni(I)] reaction process around -0.7 V. Their response towards redox reagents is almost unique. While the reactivity of **1** towards $NaBH_4$ is characterized by a substrate saturation process [k_{obs} = 8.4 x 10^{-3} s^{-1}; $\Delta S^{\neq}$ = -198.5 J mol^{-1} deg^{-1}], the corresponding reactivity profile of **2** is essentially a one-step process, associated with essentially three isosbestic points [k_{obs} = 9.0 x 10^{-3} s^{-1}; $\Delta S^{\#}$ = -186.0 J mol^{-1} deg^{-1}]. The related $NaBH_4$ reduced complexes [**1R** and **2R**] could be isolated in the solid state as dark-colored, hygroscopic compounds and characterized to be Ni(I) complexes with 7, 8-dihydro form of the pterin ligand residue. **1R** and **2R** respond differently towards a reaction mixture of bromobenzene/O_2; reaction profile of the latter is characterized by two isosbestic points. Their k_{obs} and $\Delta S^{\neq}$ values are in the range 1.4 x

10^{-2} to 8.8 x 10^{-3} s^{-1} and -191.6 to -178.0 J mol^{-1} deg^{-1}, respectively, consistent with a group transfer process, involving associative pathway. Stoichiometric studies could establish the isolation of 4-bromophenol in each case, indicating activation of the aromatic ring. The above reactivity data highlight the change over in reaction profile brought about by substituting the aquo group of **1** with an imidazole group in **2**, that is, the fine tuning of both metal and pterin-centred redox reactivities. No less interesting is the oxidation of **2R** by $K_3[Fe(CN)_6]$, where the relatively better resolved reaction profile is marked by three isosbestic points [k_{obs} = 3.6 x 10^{-2}; $\Delta S^{\neq}$ = -184.0 J mol^{-1} deg^{-1}]. The above ability of facile reactions with either a reducing agent ($NaBH_4$) or an oxidizing agent [bromobenzene/O_2 mixture or $K_3[Fe(CN)_6]$], may be considered as redox amphoteric behavior; electronic structures (DFT) provide with the necessary frame work for rationalizing this property.

Introduction

Nickel (relative atomic mass = 58.69) is a first-row transition metal in group VIII B of the periodic table. It can exist in oxidation states from 0 to +4 and all but the +4 state have been observed in biology. As per the relevant Frost diagram, only small free energy barriers could separate the lower oxidation states (0, +1 and +2) and thereby allowing their facile change over. The nickel enzymes can be divided into two groups: redox enzymes and hydrolases. The five nickel redox enzymes are hydrogenase, CO dehydrogenase (CODH), acetyl-CoA synthase (ACS), methyl-coenzyme M reductase (MCR) and superoxide dismutase (SOD). Glyoxalase –I and urease are Ni hydrolases. Ni proteins that are not enzymes, are also known.[103,104] These include regulatory proteins (NikR) and chaperonius and metal uptake proteins (CooJ, CooE, UreE and ABC transporters).

Although the 2+ state ($3d^8$) is most common, the Ni redox enzymes appear to access either the 2+/1+ and/ or the 3+/2+ redox couples. It has been proposed that the 0 state is important during catalysis by acetyl-CoA synthase. The hydrolases appear to only use Ni^{2+}, which is a Lewis acid. Since Ni^{+} and Ni^{3+} are paramagnetic, EPR spectroscopy is a valuable probe for studying Ni redox enzymes. Some Ni enzymes have rather strong UV-visible and magnetic circular dichroism (MCD) bands that are redox- and coordination-dependent.

The present redox non-innocent pterin ligand 7-methypterin-6-carboxylic acid (H_2L) provides with an opportunity to explore the coordination chemistry of nickel, in at least a couple of its biologically relevant oxidation states. A σ-donor ancillary ligand like 1, 2-diaminoethane (en) helps to quench the Lewis acidity of the Ni^{2+} centre at least partly, so that the coordinating influence of the pterin ligand can prevail here. The imidazole ligand provides with further modulation of the nickel-pterin-en coordination environment. The above ligand combinations allow to grow x-ray quality crystals of the relevant complexes from the aqueous alkaline medium. Such complexes with redox active metal and pterin centres are excellent candidates for redox reactions with well-chosen reagents. Some of the bench mark data may be regarded as biomimatic chemistry.

Experimental

Materials: Reagent grade chemicals were used as received. Solvents were purified before use following literature procedures [20]. Kinetic and electro-chemical studies were performed in spectroscopy grade SRL, Mumbai CH_3OH and DMSO respectively; Bu_4NClO_4 (TBAP) was obtained by published methods [72]. Imidazole was obtained from E.Marck, Mumbai. CD spectra were recorded on a Jasco CD spectrometer (model J-815). 7-methylpterin-6-carboxylic acid was

prepared as par the published methods [19]; it was characterized through different physico-chemical methods including elemental analysis, ESIMS, IR, UV – VIS, and ^{1}H NMR data .

Methods : Most of the physico-chemical methods of characterization were the same as that discussed in Chapters II and III. IR spectra (KBr) were recorded on a Perkin Elmer FTIR Rx1. Magnetic susceptibilities were checked with a Sherwood magnetic susceptibity balance (MSB Mk1), using $Hg[Co(SCN)_4]$ as the calibrant.

X-ray data collection: Apex2 (Bruker , 2007); cell refinement: Apex2 (Bruker , 2007); data reduction: USER DEFINED DATA REDUCTION; program(s) used to solve structure: *SHELXS* 86 (Sheldrick, 2008); program(s) used to refine structure: *CRYSTALS* (Betteridge *et al.*, 2003); molecular graphics: *CAMERON* (Watkin *et al.*, 1996); software used to prepare material for publication: *CRYSTALS* (Betteridge *et al.*, 2003).

Synthesis of the complexes

$[Ni(C_8H_5N_5O_3)(C_2H_8N_2)(H_2O)].\ 2H_2O$ (1)

The title complex was prepared by the slow addition of an aqueous alkaline solution (NaOH: 44mg, 1.1 mmol) of the pterin ligand H_2L ($C_8H_7N_5O_3$ 1.5 H_2O; MW 248) (124mg, 0.5mmol) to a well-stirred warm (323K; paraffin oil bath) aqueous reaction mixture containing $NiSO_4.\ 7H_2O$ (140mg, 0.5mmol) and 1, 2 – diaminoethane (36mg, 0.6mmol) under subdued light; final volume was 35 ml. The pH was adjusted to 9.2 and the stirring was continued for 3h. Upon standing, the reaction medium deposited yellow-brown crystals after 2 days, which were suitable for single crystal x-ray diffraction; yield, 30%. Analytically pure compound could be obtained by filtration, repeated washing with small quantities of water and drying in vacuo over silica gel. Analysis, calculated for $C_{10}H_{19}N_7O_6Ni$: C 30.70, H 4.89, N 25.06 %; found: C 30.51, H 5.11, N 24.55 %. UV – VIS absorption bands [CH_3OH, $\lambda_{max}^{nm}(\log\epsilon)$]: 205(4.91), 233sh(4.35), 277(4.44),

349(4.21), 734(1.24), 893(1.90)

$[Ni(C_8H_5N_5O_3)(C_2H_8N_2)(C_3N_2H_4)].\ 2H_2O$ (2)

The title complex was synthesized by the dropwise addition of an aqueous alkaline solution (NaOH: 11mg, 0.275 mmol) of the pterin ligand (31mg, 0.125mmol) to a warm (311K; paraffin oil bath) aqueous reaction mixture containing $NiSO_4.\ 7\ H_2O$ (35mg, 0.125mmol), 1,2 – diaminoethane (7.5mg, 0.125mmol) and 1H – imidazole (14mg, 0.2mmol); final volume was 45ml. The pH was adjusted to 10.3 and the mixture was stirred for 3h; final pH was 9.3. The orange coloured solution was transferred to a 100ml beaker and allowed to stand at room temperature. Orange crystal appeared after 4 days which were suitable for single crystal x-ray diffraction; yield, 40%. Sample for analytical purpose could be obtained by filtration, repeated washing with small quantities of water and drying in vacuo over silica gel. Analysis, calculated for $C_{13}H_{21}N_9O_5Ni$: C 35.31, H 4.80, N 28.52%; found: C 35.72, H 4.70, N 28.07%. UV – VIS absorption bands [CH_3OH, $\lambda_{max}^{nm}(\log\epsilon)$]: 270(4.26), 369(3.88), 542br(1.12), 620br(0.96), 698(1.21), 748(1.24), 812(1.43), 921br(0.88), 1063sh(1.32)

Synthesis of $Na[Ni^{I}(L')(en)(H_2O)].\ 2H_2O.CH_3OH$ (1R), where $(L')^{2-}$ is the 7,8-dihydro form (Scheme II-4) of the pterin ligand anion (Scheme II-1), as established on the basis of microanalytical and spectroscopic data (vide infra). A methanolic solution (50 mL) of **1** (19.6 mg, 0.05 mmol) was treated with $NaBH_4$ (11.3 mg, 0.3 mmol) and the reaction was allowed to continue for 45 min at 301-303K under subdued light in a chlenk flask attached to a paraffin oil bubbler. The reaction mixture passed through a sequence of color changes e.g., yellow green → dark brown colour . It was then rotavapped and a dark brown solid was recovered. It was washed quickly (decantation) with dinitrogen purged CH_3OH (3 X 4 mL) and dried in vacuo over silica

gel for 48h.Yield: 40%. Anal. Calcd for $NaNiC_{11}H_{25}N_7O_6$: C, 31.98; H, 6.05; N, 23.74. Found: C,30.29; H, 5.65; N, 24.15.

Synthesis of Na[Ni ^{I}(L′)(en) (Im)]. $3H_2O$. (**2R**), A methanolic solution (50 mL) of **1** (22.10 mg, 0.05 mmol) was treated with $NaBH_4$ (11.3 mg, 0.3 mmol) and the reaction was allowed to continue for 45 min at 301-303K under subdued light in a Schlenk flask attached to a paraffin oil bubbler. The reaction mixture passed through a sequence of color changes e.g., yellow green → dark brown colour . It was then rotavapped and a dark brown solid was recovered. It was washed quickly (decantation) with dinitrogen purged CH_3OH (3 X 4 mL) and dried in vacuo over silica gel for 48h.Yield: 38%. Anal. Calcd for $NaNiC_{13}H_{25}N_9O_6$: C, 32.18; H, 5.15; N, 25.99. Found: C,31.45; H, 4.65; N, 24.23.

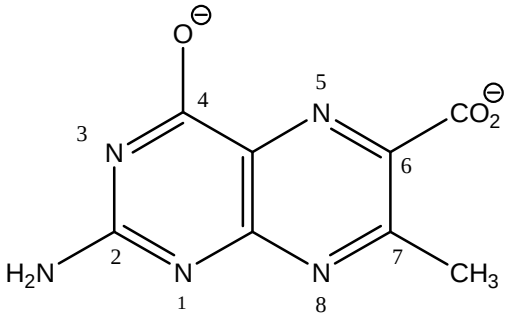

The pterin ligand (H_2L) anion (L^{2-}, $C_8H_5N_5O_3$)

Scheme IV-1

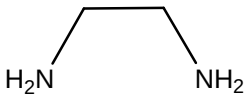

1, 2-diaminoethane (en, $C_2H_8N_2$)

Scheme IV-2

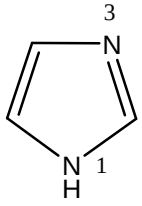

1H-imidazole (Im, $C_3N_2H_4$)

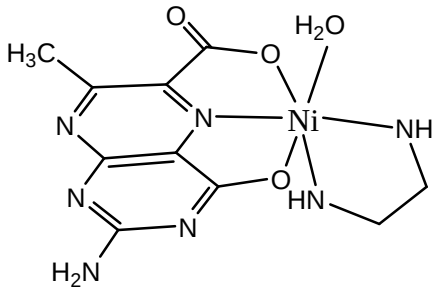

1

Scheme IV-3

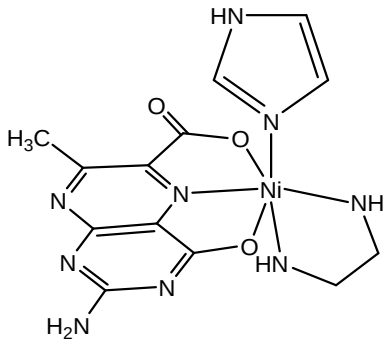

2

Scheme IV-4

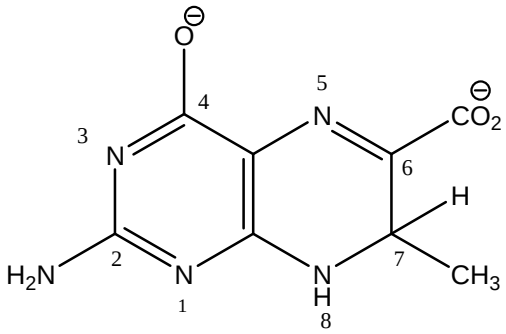

7, 8-dihydro pterin anion (L' $^{2-}$)

Scheme IV-5

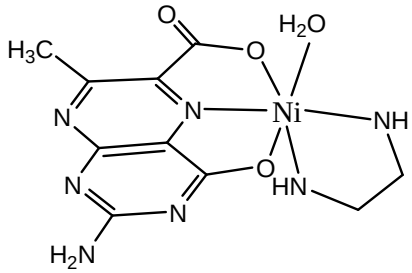

1

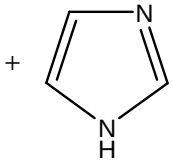

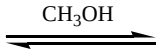

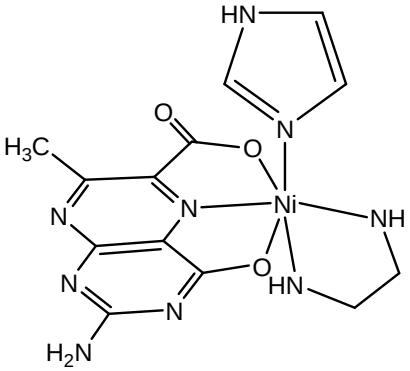

2

Scheme IV-6

Scheme IV-7

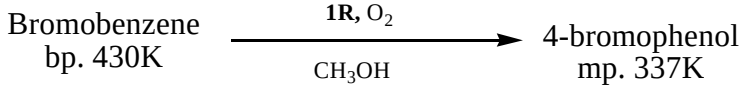

Scheme IV-8

Results and discussion

The two Ni(II) mixed ligand complexes of the ptrerin ligand (Scheme: IV-1) could be synthesized and crystallized out of the aqueous alkaline medium. The reaction conditions were

carefully controlled, including heating on a paraffin oil bath. In each case, x-ray quality crystals were deposited from the reaction medium. After proper washing and drying such crystals, analytically pure samples could be obtained giving correct microanalytical data as well as electrospray ionization mass spectral data (ESIMS). Successful use of aqueous medium for the above purpose, lends credebility to the present complexes for studies as model systems. Examples of quaternary complexes like **2**, are still rare in pterin coordination chemistry. Schemes IV-1 to IV-5 represent the present ligands and the new Ni(II) complexes.

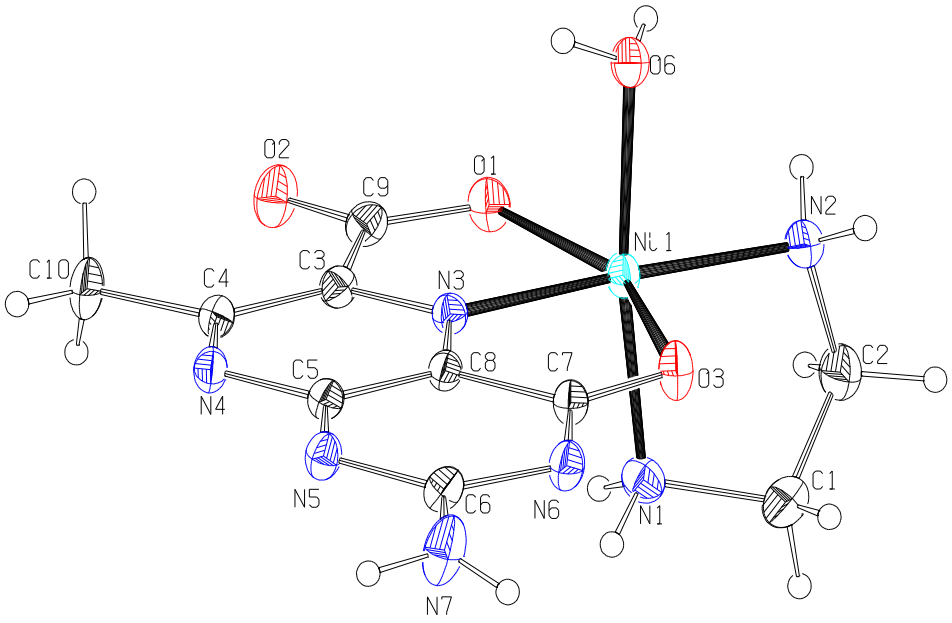

Figure IV-1. ORTEP diagram of the complex **1** with atom numbering scheme (40% probability factor for the thermal ellipsoids); lattice water molecules are omitted for clarity.

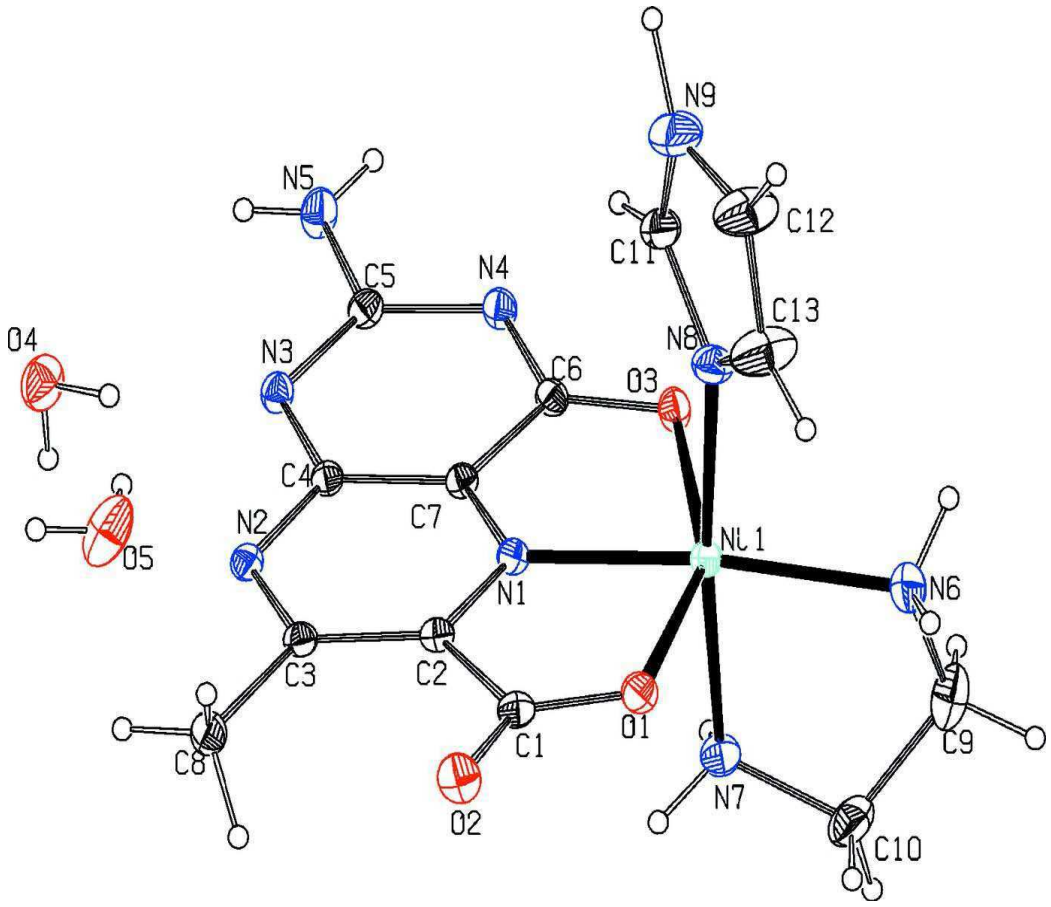

Figure IV-2. ORTEP diagram of the complex **2** with atom numbering scheme(40% probability factor for the thermal ellipsoids).

Table IV-1. Crystallographic data and structure refinement for 1 and 2

Identification code	**1**	**2**
Empirical formula	$C_{10}H_{19}N_7NiO_6$	$C_{13}H_{21}N_9NiO_5$
Formula weight	392.01	442.08
Temperature/K	293	293
Crystal system	Monoclinic	orthorhombic
Space group	$P2_1/c$	Pbcn
a/Å	10.406(4)	13.484(2)
b/Å	14.323(5)	8.8741(15)
c/Å	10.450(4)	29.959(5)
α/°	90	90
β/°	93.294(6)	90
γ/°	90	90
Volume/$Å^3$	1554.9(10)	3584.8(10)
Z	4	8
$\rho_{calc}g/cm^3$	1.675	1.638
μ/mm^{-1}	1.294	1.132
F(000)	816.0	1840.0
Crystal size/mm^3	0.490 × 0.380 × 0.280	0.240 × 0.240 × 0.030
Radiation	Mo Kα (λ = 0.71073)	Mo Kα (λ = 0.71073)

2Θ range for data collection/°	3.92 to 56.382	2.718 to 56.6°
Index ranges	$-13 \leq h \leq 13, -18 \leq k \leq 15, -11 \leq l \leq 13$	$-17 \leq h \leq 17, -11 \leq k \leq 11, -24 \leq l \leq 38$
Reflections collected	8393	19640
Independent reflections	3488 [$R_{int} = 0.035$]	4245[R(int) = 0.030]
Data/restraints/parameters	3488/0/217	4245/0/253
Goodness-of-fit on F^2	0.914	0.945
Final R indexes [I>=2σ (I)]	$R_1 = 0.0499$, $wR_2 = 0.1255$	$R_1 = 0.0365$, $wR_2 = 0.0887$
Final R indexes [all data]	$R_1 = 0.0638$, $wR_2 = 0.1347$	$R_1 = 0.0442$, $wR_2 = 0.0921$
Largest diff. peak/hole / e $Å^{-3}$	1.10/-0.84	0.62/-0.32

Table IV- 2. Geometric parameters for (1)

Bond lengths

Atom	Atom	Length/Å	Atom	Atom	Length/Å
Ni1	O1	2.120(2)	C8	C7	1.460(4)
Ni1	N3	1.977(3)	C5	N4	1.362(4)
Ni1	O3	2.325(2)	C5	N5	1.358(4)
Ni1	O6	2.125(2)	N4	C4	1.349(4)
Ni1	N1	2.074(3)	C4	C10	1.501(4)

Ni1	N2	2.065(3)	N5	C6	1.360(4)
O1	C9	1.288(4)	C6	N6	1.381(4)
C9	O2	1.239(4)	C6	N7	1.347(4)
C9	C3	1.526(4)	N6	C7	1.338(4)
C3	N3	1.339(4)	C7	O3	1.274(4)
C3	C4	1.416(4)	N1	C1	1.479(5)
N3	C8	1.325(4)	C1	C2	1.501(5)
C8	C5	1.401(4)	C2	N2	1.481(5)

Bond angles

Atom	Atom	Atom	Angle/˚	Atom	Atom	Atom	Angle/˚
O1	Ni1	N3	77.20(10)	Ni1	N3	C8	119.14(19)
O1	Ni1	O3	153.50(8)	N3	C8	C5	121.5(3)
N3	Ni1	O3	76.31(9)	N3	C8	C7	117.4(3)
O1	Ni1	O6	88.63(9)	C5	C8	C7	121.0(3)
N3	Ni1	O6	93.13(10)	C8	C5	N4	119.9(3)
O3	Ni1	O6	92.06(9)	C8	C5	N5	120.5(3)
O1	Ni1	N1	95.49(11)	N4	C5	N5	119.6(3)
N3	Ni1	N1	94.14(11)	C5	N4	C4	117.9(3)
O3	Ni1	N1	87.16(10)	C3	C4	N4	121.6(3)
O6	Ni1	N1	172.29(10)	C3	C4	C10	122.5(3)
O1	Ni1	N2	103.49(11)	N4	C4	C10	115.9(3)

N3	Ni1	N2	177.56(11)	C5	N5	C6	114.6(2)
O3	Ni1	N2	103.02(10)	N5	C6	N6	129.2(3)
O6	Ni1	N2	89.23(10)	N5	C6	N7	116.3(3)
N1	Ni1	N2	83.47(11)	N6	C6	N7	114.4(3)
Ni1	O1	C9	115.51(19)	C6	N6	C7	116.6(2)
O1	C9	O2	124.2(3)	C8	C7	N6	117.8(3)
O1	C9	C3	115.2(3)	C8	C7	O3	118.1(3)
O2	C9	C3	120.6(3)	N6	C7	O3	124.1(3)
C9	C3	N3	111.1(3)	Ni1	O3	C7	108.99(19)
C9	C3	C4	129.8(3)	Ni1	N1	C1	106.5(2)
N3	C3	C4	119.1(3)	N1	C1	C2	108.5(3)
C3	N3	Ni1	120.9(2)	C1	C2	N2	109.2(3)
C3	N3	C8	120.0(3)	C2	N2	Ni1	109.3(2)

Table IV- 3. Hydrogen Bonds Geometry for 1

D	H	A	D-H-A/°	d(D-H)/Å	d(H-A)/Å	d(D-A)/Å
N7	H172	O5[1]	130.79(11)	0.871	2.588	3.226(5)
N7	H171	O2[2]	120.55(12)	0.847	2.370	2.894(5)
O6	H182	N5[1]	147.64(10)	0.838	2.061	2.805(5)
O6	H181	O4	170.64(11)	0.821	1.962	2.775(5)
N2	H221	O4	137.51(11)	0.872	2.401	3.100(5)

N2	H222	O6[3]	175.94(9)	0.847	2.218	3.064(5)
N1	H192	O1[4]	146.50(8)	0.892	2.391	3.173(5)
N1	H192	O2[4]	154.36(9)	0.892	2.416	3.242(5)
O4	H231	O3[3]	160.21(11)	0.828	1.891	2.684(5)
O4	H232	O5[5]	170.85(13)	0.821	2.043	2.857(5)
O5	H242	O1	160.40(10)	0.833	2.213	3.010(5)

Table IV- 4. Geometric parameters for 2

Bond Lengths

Atom	Atom	Length/Å	Atom	Atom	Length/Å
Ni1	N1	1.9790(16)	N7	C10	1.468(3)
Ni1	N6	2.0801(19)	N8	C11	1.337(3)
Ni1	N7	2.0956(17)	N8	C13	1.339(3)
Ni1	N8	2.0640(17)	N9	C11	1.343(3)
Ni1	O1	2.1522(14)	N9	C12	1.352(4)
Ni1	O3	2.2725(14)	O1	C1	1.270(2)
N1	C2	1.324(2)	O2	C1	1.243(2)
N1	C7	1.320(2)	O3	C6	1.270(2)
N2	C3	1.338(2)	C1	C2	1.522(3)
N2	C4	1.358(2)	C2	C3	1.418(3)
N3	C4	1.349(2)	C3	C8	1.498(3)

N3	C5	1.351(2)	C4	C7	1.396(2)
N4	C5	1.373(2)	C6	C7	1.453(2)
N4	C6	1.332(2)	C9	C10	1.491(4)
N5	C5	1.332(3)	C12	C13	1.329(4)
N6	C9	1.467(3)			

Bond Angles

Atom	Atom	Atom	Angle/˚	Atom	Atom	Atom	Angle/˚
N1	Ni1	N6	173.25(7)	Ni1	O3	C6	108.71(11)
N1	Ni1	N7	91.67(7)	O1	C1	O2	125.26(18)
N1	Ni1	N8	94.18(7)	O1	C1	C2	114.90(16)
N1	Ni1	O1	75.91(6)	O2	C1	C2	119.82(17)
N1	Ni1	O3	77.49(6)	N1	C2	C3	118.47(16)
N6	Ni1	N7	82.05(8)	C1	C2	N1	111.47(16)
N6	Ni1	N8	92.13(8)	C1	C2	C3	130.06(16)
N6	Ni1	O1	101.53(7)	N2	C3	C8	116.27(17)
N6	Ni1	O3	105.07(7)	C2	C3	N2	121.72(16)
N7	Ni1	N8	174.12(7)	C2	C3	C8	122.00(17)
N7	Ni1	O1	90.31(7)	N2	C4	N3	120.48(16)
N7	Ni1	O3	91.93(6)	N2	C4	C7	119.28(16)
N8	Ni1	O1	91.64(7)	N3	C4	C7	120.24(16)
N8	Ni1	O3	88.81(7)	N3	C5	N5	116.89(17)

O1	Ni1	O3	153.36(5)	N4	C5	N3	128.64(17)
Ni1	N1	C2	121.70(13)	N4	C5	N5	114.46(17)
Ni1	N1	C7	117.63(12)	N4	C6	O3	123.89(16)
C2	N1	C7	120.57(16)	N4	C6	C7	117.18(16)
C3	N2	C4	118.22(16)	O3	C6	C7	118.90(16)
C4	N3	C5	115.13(16)	C4	C7	N1	121.64(16)
C5	N4	C6	117.22(16)	C6	C7	N1	117.14(16)
Ni1	N6	C9	109.21(15)	C6	C7	C4	121.22(16)
Ni1	N7	C10	108.07(14)	N6	C9	C10	108.2(2)
Ni1	N8	C11	128.23(15)	C9	C10	N7	109.3(2)
Ni1	N8	C13	126.84(17)	N9	C11	N8	111.0(2)
C11	N8	C13	104.8(2)	N9	C12	C13	107.4(2)
C11	N9	C12	105.9(2)	N8	C13	C12	110.7(2)
Ni1	O1	C1	115.81(12)				

Table IV- 5. Hydrogen Bonds Geometry for 2

D	H	A	D-H-A/°	d(D-H)/Å	d(H-A)/Å	d(D-A)/Å
N6	H62	O5[1]	151.75(7)	0.900	2.276	3.099(3)
N7	H72	N2[2]	176.41(5)	0.899	2.400	3.298(3)
N7	H71	O4[2]	135.18(6)	0.899	2.509	3.211(3)
N5	H51	N4[3]	177.50(15)	0.848	2.136	2.983(3)

O5	H51	$O2^{4}$	175.53(8)	0.857	1.967	2.822(3)
N5	H52	O4	140.01(15)	0.778	2.559	3.194(3)
O5	H52	$O1^{5}$	146.29(7)	0.737	2.148	2.791(3)
N9	H91	$O5^{6}$	160.29(15)	1.055	2.003	3.017(3)
C12	H121	$O2^{6}$	137.67(9)	0.931	2.186	2.941(3)
O4	H42	N3	169.81(7)	0.852	1.994	2.837(3)
O4	H41	$O3^{7}$	163.23(6)	0.866	2.018	2.858(3)

Molecular structures of $[Ni(C_8H_5N_5O_3)(C_2H_8N_2)(H_2O)].\ 2H_2O$ (1) and $[Ni(C_8H_5N_5O_3)(C_2H_8N_2)(C_3N_2H_4)].\ 2H_2O$ (2)

Figure IV-1 and Figure IV-2 represent the molecular structures of the above complex compounds. Their crystallographic data and structure refinements are shown in Table IV-1. The geometric parameters and hydrogen bonding data of **1** are presented in Table IV-2 and Table IV-3 respectively. Table IV-4 and Table IV-5 represent the geometric parameters and hydrogen bonds data of compound **2**. For complex **1** the six – coordinated Ni (II) atom shows departure from a regular octahedral geometry with respect to both bond lengths and bond angles (Figure IV-1, Table IV-2). The basal plane is formed by the two nitrogen atoms (N1, N2) of en, the pyrazine ring nitrogen atom (N3) of the pterin ligand and the aqua group oxygen atom (O6). The axial positions are occupied by the two pterin oxygen atoms O1 and O3, with the latter one forming the longest axial bond [2.325 (2) Å]. One important factor causing distortion from regular octahedral geometry is that this pterin ligand forms two five-membered chelate rings with small bite angles (76.31^0 and 77.14^0), instead of only one per pterin ligand for the earlier case (Crispini *et al.*, 2005)[83]. A perusal of the charge balance of this complex, indicates that this

pterin ligand acts as a binegative tridentate ONO donor. An orthogonal disposition of the en and pterin chelate rings is observed which helps to minimize the steric repulsion. Of the three axes, least deviation from linearity is observed in the N3 – Ni1 – N2 direction (177.52^0) where the highest electron density is concentrated [Ni1 – N3: 1.977 (2) Å; Ni1 – N2: 2.065 (3) Å]. It represents the unique combination of a σ – donor atom N2 (en) and the N3 atom of the redox noninnocent pterin ligand from the opposite directions of the Ni (II) centre (d^8), with possible assistance from the π – donating phenolate and carboxylate oxygen atoms (Kohzuma *et al.*, 1988)[18a]. Again, location of the pyrazine ring nitrogen atom (N3) in the basal plane is consistent with the earlier observations on related copper complexes (Odani *et al.*, 1992).[84]

Although the exocyclic bond length data of the pyrazine ring, e.g., C3 – C9 [1.527 (4)Å] and C4 – C10 [1.503 (4)Å] reflect only limited conjugation with the pyrazine ring π system, the corresponding bond length data of the pyrimidine ring, e.g., C7 – O3 [1.267 (3)Å] and C6 – N7 [1.349 (4)Å] merit attention. Small deviations, e.g., 2.02^0 and 1.37^0 of the C7/N6/C6 and C5/N5/C6 segments respectively, with respect to the C – N7 multiple bond, indicate near planarity for the pyrimidine ring. So it can participate in the electron shuffling process by the pterin moiety from the pyrazine ring N4 to the C7 – carbonyl group, as suggested by Joule and coworker (Beddoes *et al.*, 1993; Russell *et al.*, 1992).[22,23] Formation of the Ni1 – O3 bond assists this process.In the crystal, the complex molecules and lattice water molecules are linked by inter-molecular N – H⋯.O, O – H⋯.N and O – H·Ɵ hydrogen bonds (Table IV-3). The lattice water molecules are decisive for the crystal packing (Figure IV-3)

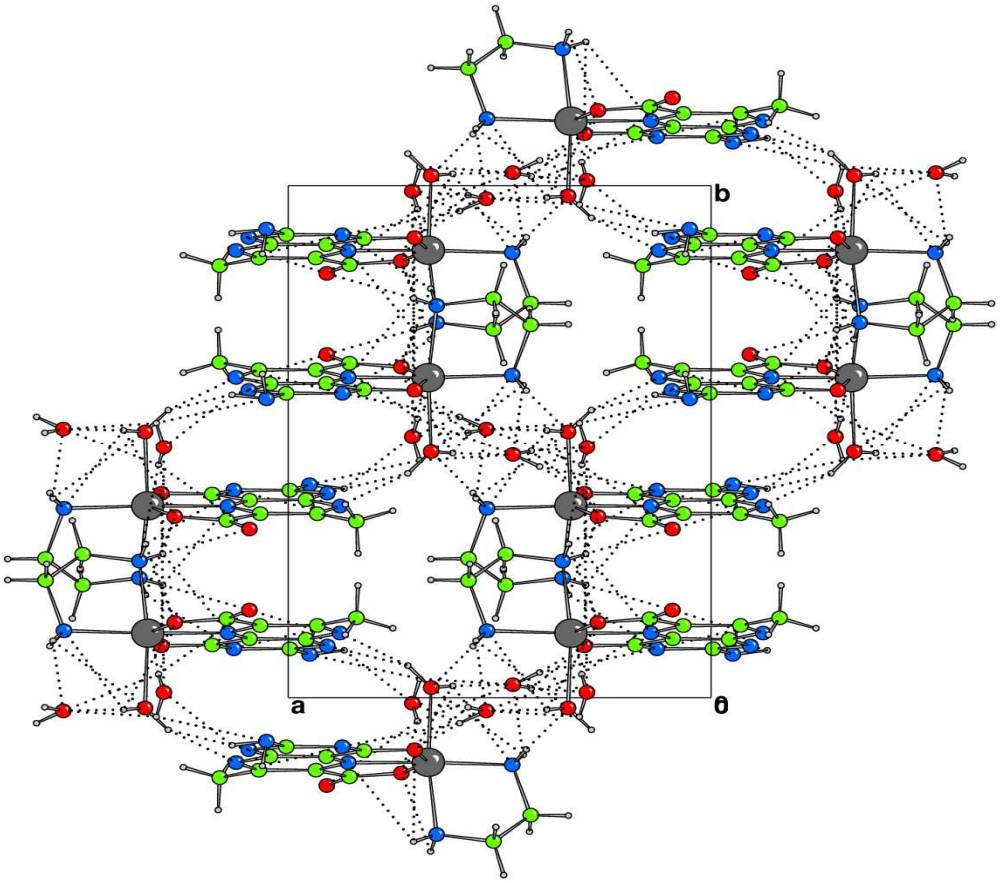

Figure IV-3. Crystal packing diagram of **1** and H-bonding network viewed along c axis.

The molecular structure of complex **2** is shown in Figure IV-2. Here a tridentate 2-amino-7 –methyl-4- oxidopteridine- 6- carboxylate ligand, a bidentate ancillary ethane-1, 2- diamine (en) ligand and a monodentate 1H – imidazole (im) ligand complete a distorted octahedral geometry around the Ni(II) atom. The two N atoms (N6 and N7) of en, a pyrazine ring N atom (N1) of the pterin ligand and an imidazole ring N atom (N8) forming the equatorial plane. The two pterin O atoms (O1 an O3) occupy the longer axial positions, with the phenolate O3 constituting the longest axial bond [2.2725(14) Å]. As compared to complex **1** , an unique situation is presented by complex **2** (Figure IV-2) where the equatorial plane is formed by four

nitrogen atoms. The pterin ligand forms two five-membered chelate rings having small bite angles [75.91(6)^0 and 77.50(6)^0], instead of only one per pterin ligand for an earlier case (Crispini et al., 2005)[83]. This factor is responsible to a large extent for the observed distortion here from regular octahedral geometry. Accordingly, the O1 – Ni1 – O3 axis shows maximum deviation (153.37^0) from linearity. Again, closest approach to linearity (174.10^0) is observed for the N7 – Ni1 – N8 axis which is associated with both the imidazole and en ligands. Here each such ligand tries to achieve near orthogonality [angle between the imidazole ring N atom (N8) and the mean plane of the pterin ring = 91.55^0; dihedral angle between the mean plane of the en moiety and the pterin ring = 90.49^0], with respect to the pterin ligand, for minimizing the steric repulsion. . In accordance with the earlier observations on related copper complexes, the pyrazine ring N atom (N1) is located in the equatorial plane.[84] The associated short metal-ligand distance (Ni1-N1=1.9790Å) indicates dπ – pπ interaction between the pterin ring and the Ni(II) centre (d^8), with further assistance from the nearby π-donating phenolate and carboxylate O atoms [18a] The pterin ligand is coordinated in its binegative form as a ONO donor, as evident from the charge balance of this Ni(II) complex.

The significantly shorter nature of the O3 – C6 [1.271(2) Å] and N5 – C5 [1.332(2)Å] bonds could be rationalized in terms of electron – shuffling ability of the pterin ring , as discussed earlier for complex **1**.[17c, 17d, 22, 23,]In the crystal, intermolecular N – H ….N, N – H ….O,O – H…N, O – H ….O hydrogen bonds (Table IV-5) link the complex molecules and lattice water molecules into layers along the a axis (Figure IV-4). The lattice water molecules play a decisive role for the crystal packing. Presence of the imidazole ligand in the coordination sphere for **2**, leads to a denser crystal packing with Z= 8, as compared to Z= 4 for **1**. This is the

highest Z value for the present series of x-ray structurally characterized pterin coordination complexes.[17a – 17e]

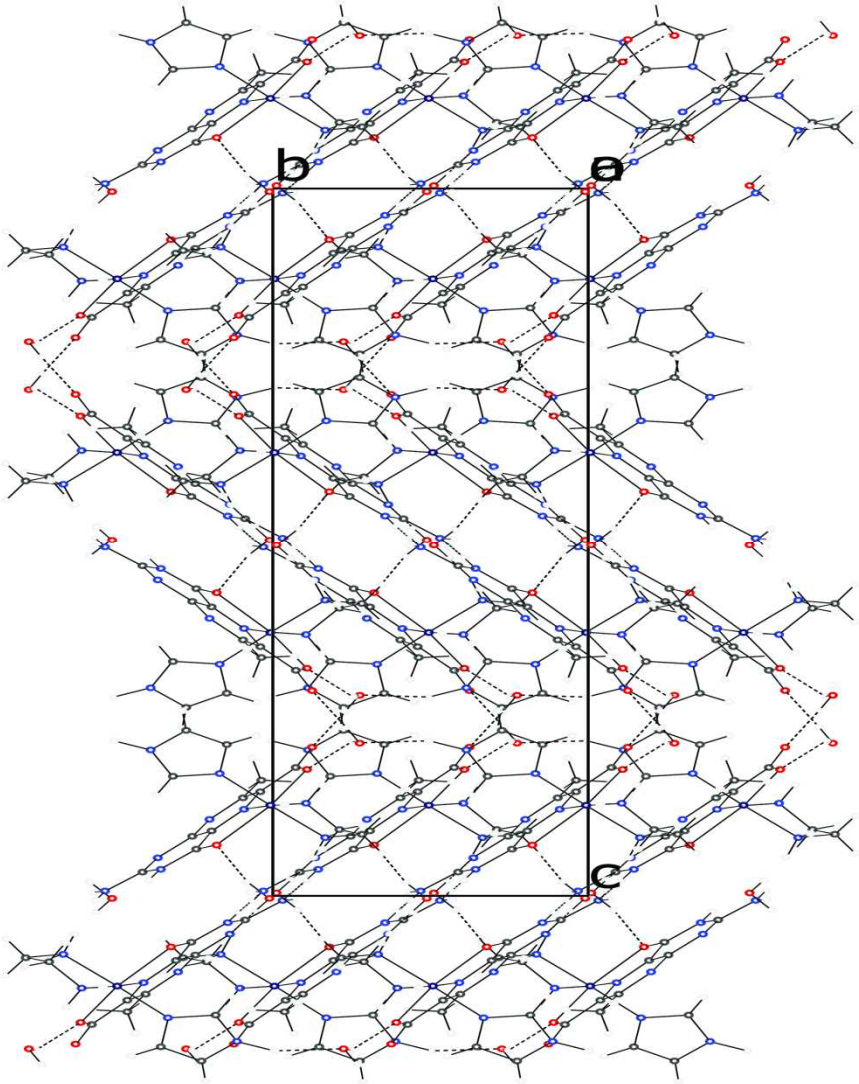

FigureIV- 4. Crystal packing diagram of **2** with H-bonding network viewed along a axis

---

Table IV-6 shows the effect of imidazole substitution on selected bond length data in terms of Δ = (**1** – **2**) values (Å); in a couple of cases, the change over in bond length data fall in the range of 0.05 – 0.06 Å. As evident from literature data such change over in dimension can affect (Table

IV-8) redox reactivity to a large extent.[79] Significance of this observation in the present context (reactivity) is elucidated later.

Table IV- 6. Effect of imidazole substitution on selected bond length data.

Sl No.	Bond	Bond length on **1** (Å)	Bond length on **2** (Å)	Δ=(**1** – **2)** value (Å)
1	Ni1 – O1	2.120(2)	2.1522(14)	-0.0322
2	Ni1 – O2	2.325(2)	2.2725(14)	0.0525
3	Ni1 – N1	2.074(3)	2.0956(17)	-0.0216
4	Ni1 – N2	2.065(3)	2.0801(19)	-0.0151
5	Ni1 – N3	1.977(3)	1.9790(16)	-0.002
6	Ni1 - X	2.125(2)	2.0640(17)	0.061

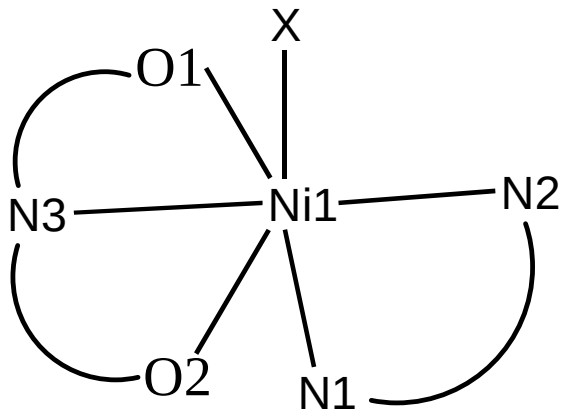

1 (X=H_2O) [**Figure IV-1**.]

2 (X = Im) [**Figure IV-2**.]

N.B. O1, N3 and O2 as shown above, correspond to O6, N5 and O4 donor atoms of the pterin ring (**Scheme IV-1**)

ESIMS Data

Electronspray ionization mass spectrometry has been utilized as a soft ionization technique for the characterization of different types of inorganic and coordination compound including metal clusters;[77] the assignment of molecular formula (or any definite fragment resulting from it) is confirmed by the experimental value of m/z (most abandoned isotopic mass) as well as matching between the experimental and simulated (calculated) isotopic distribution profile.[24,78] Characterization of the desolvated species from a coordination compound in the mass spectrum is well established; even the presence of a fragmentation peak associated with loss of one of the ligand is taken as evidence in favour of a molecular ion peak.[86] Sometimes, isotope peak may be more intense then the calculated value because of ion-molecule interactions that vary with the sample concentration or with the class of compound involved e.g., the transfer of a hydrogen atom from the excess of the compound to the molecular ion in some cases.[21] Figure IV-5 shows the ESIMS data of **1** where the peak at m/z 338 corresponds to the dehydrated species $[Ni(L)(en)]^+$; the m/z value (most abandoned isotopic mass) and the isotope distribution profile agreed with the corresponding theoretical value, thereby supporting the chemical composition of **1**, in conjunction with the elemental analysis and x-ray structural data.[24] Figure IV-6(a) shows another fragment peak at m/z = 278 corresponding to the species $[Ni(L)]^+$, obtained through loss of the ancillary ligand (en) as well as the intra/extra spheric water molecules; Figure IV-6(b) shows the corresponding calculated isotope distribution profile.[24]

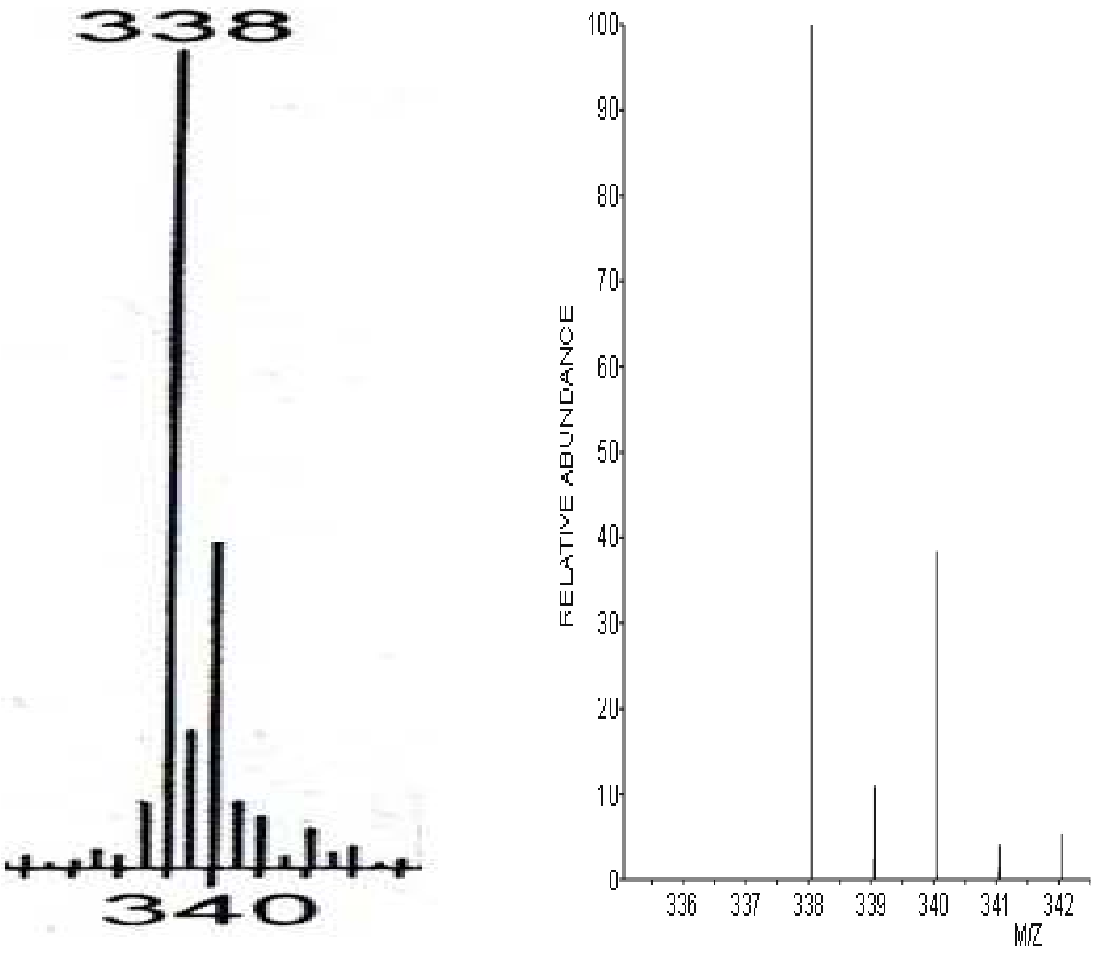

(a) (b)

Figure IV-5. (a) ESIMS data of **1**; (b) the calculated isotope pattern for the base peak at m/z = 338 corresponding to the fragment $[Ni(L)(en)]^+$

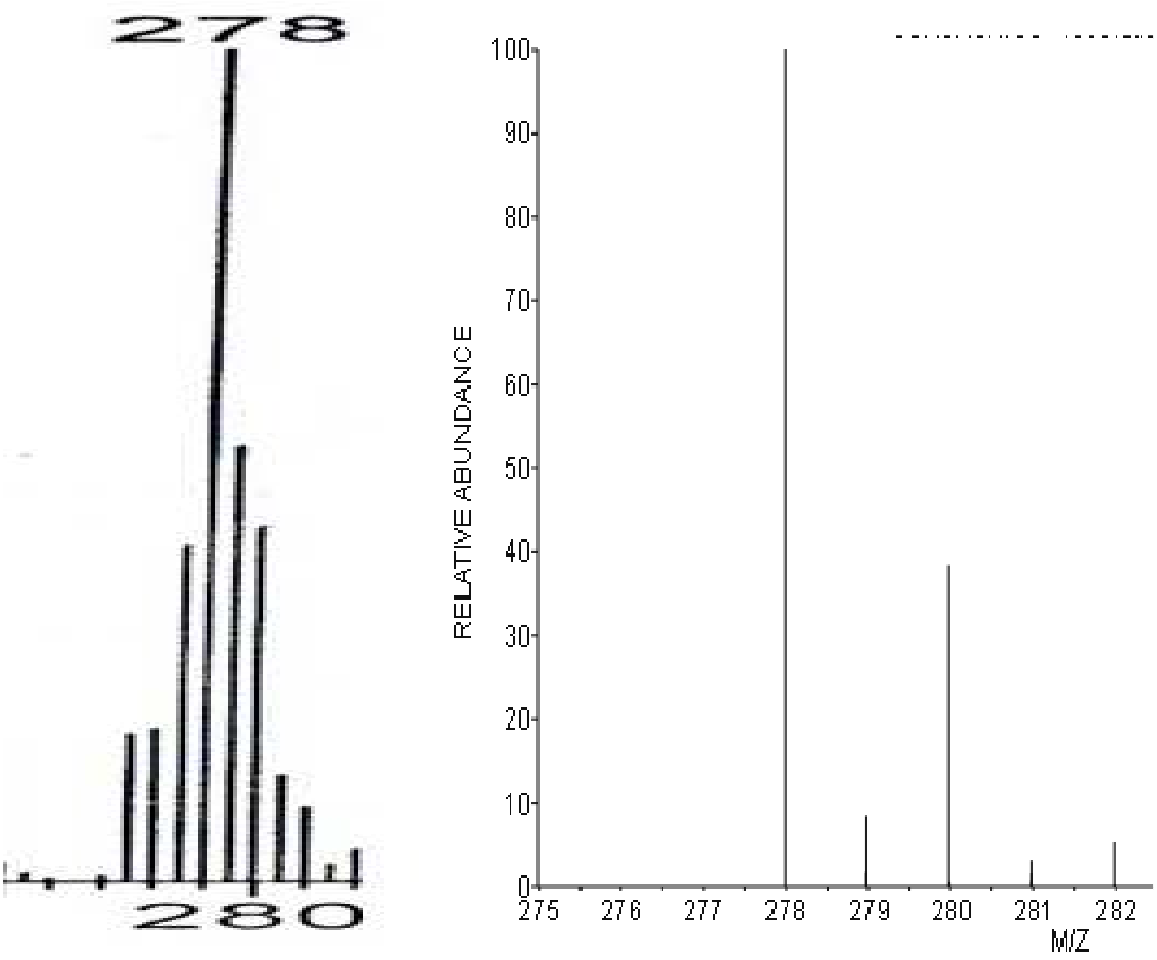

(a) (b)

Figure IV- 6. (a) ESIMS data of **1**; (b) the calculated isotope pattern for the base peak at m/z = 278 corresponding to the fragment $[Ni(L)]^+$.

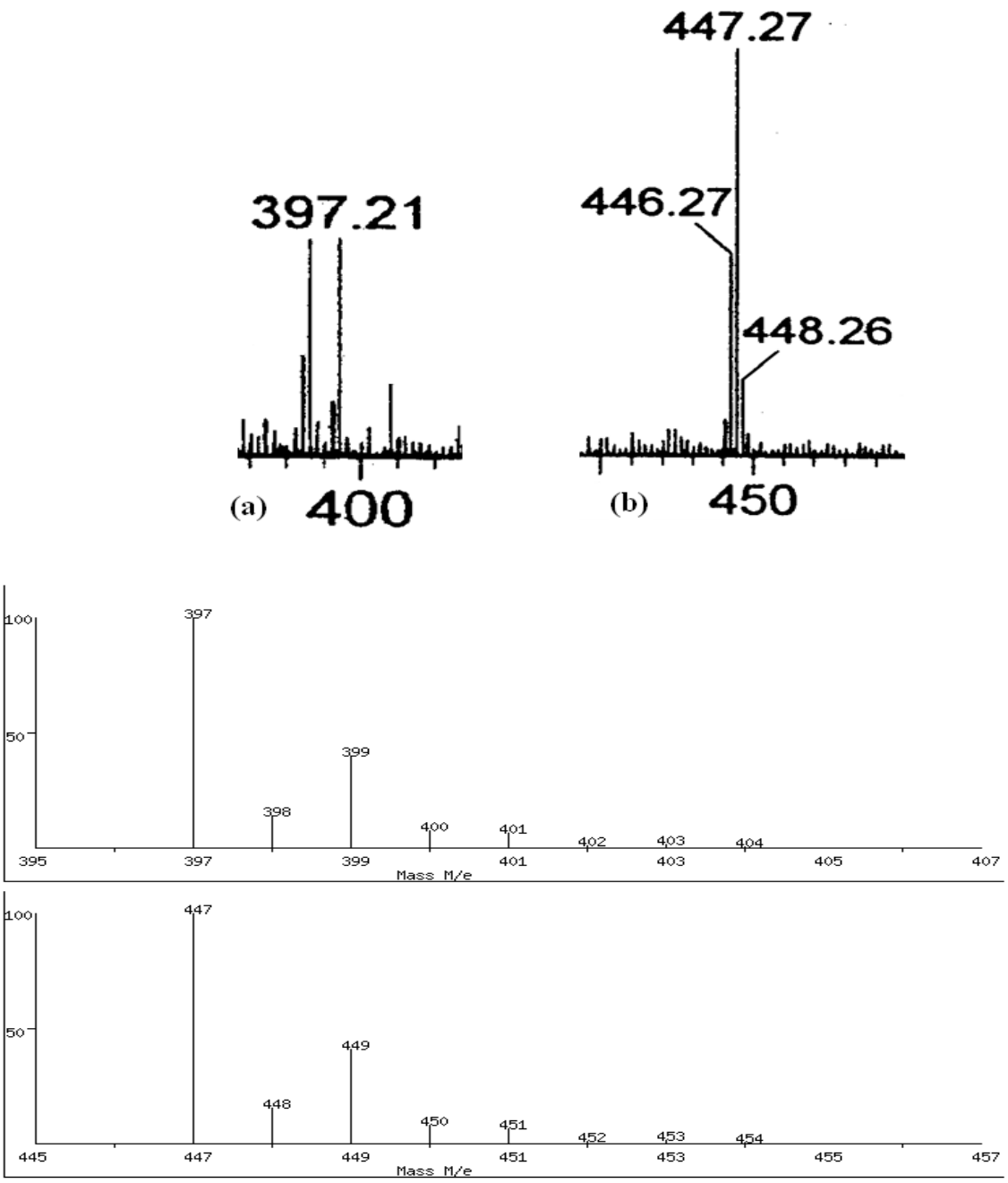

Figure IV- 6a. (a) ESIMS data of **1R**; the calculated isotope pattern for the base peak at m/z = 447.27 and 397.1 .

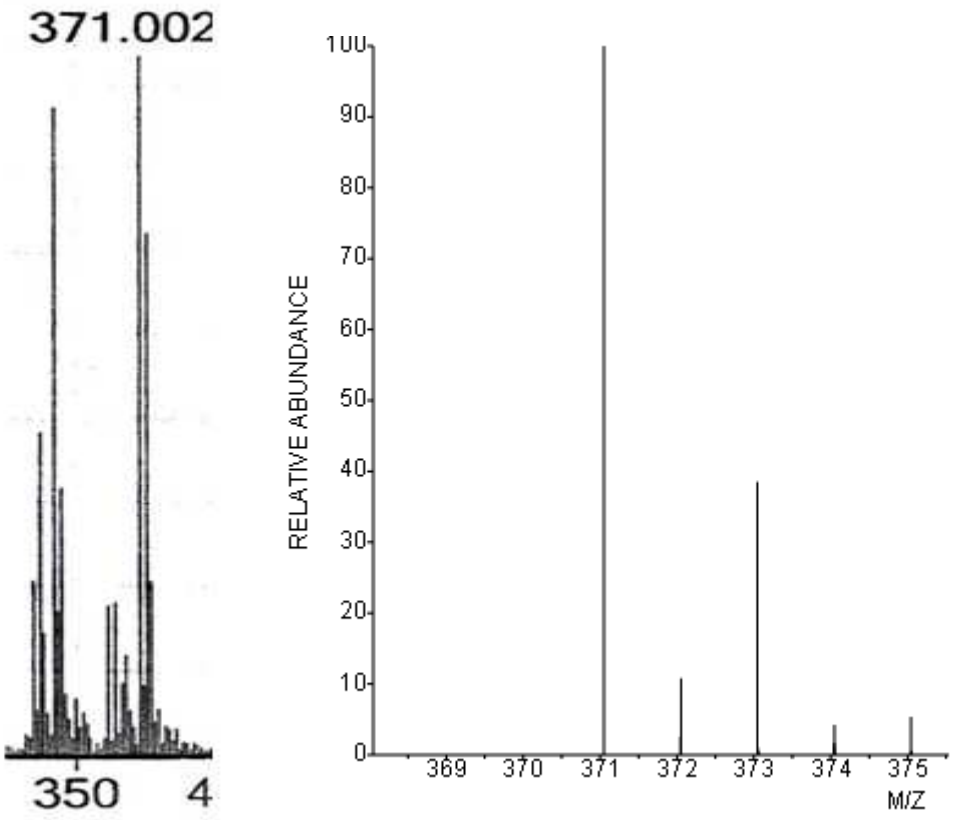

(a) (b)

Figure IV-7. (a) ESIMS data of **2**; (b) the calculated isotope pattern for the base peak at m/z = 371 corresponding to the fragment $[M\text{-}Im\text{-}3H^{+}]^{+}$, where M is the molecular formula of **2**.

The above mass spectral data verify the architectural stability of this mononuclear mixed ligand Ni(II) complex as well as the strength of the Ni(II)-pterin bonding.[77,78] Figure IV-7(a) shows the ESIMS data of **2** indicating a peak at m/z 371, corresponding to the fragment $[M\text{-}Im\text{-}3H]^{+}$; its isotope distribution pattern could be calculated [Figure IV-7(b)] . Once again the stability of the Ni(II) – pterin as well as the Ni(II) – en bonding is demonstrated, along with the affinity of the

extraspheric H_2O molecule, as evident from the crystal packing diagram (Figure IV-4). In other words, the neutral monodentate ligand (Im) can be lost from this quaternary complex **2**, without affecting its overall stability.

ESIMS data of 1R

The ESIMS data of **1R** is shown in Figure IV-6a . The molecular ion peak $[M - 1]^+$ is observed at m/z 447.27 where M is the molecular formula of **1R** with its full complement of extraspheric solvent molecules. It verifies the architectural stability of **1R** possessing the 7, 8-dihydro form of the pterin ligand residue (L'^{2-}, Scheme IV- 6) along with a Ni(I) centre and a balancing Na^+ counter ion. Another peak is observed at m/z 397.1 which corresponds to the fragmant $[M\text{-}CH_3OH - H_2O - 1]^+$, once again verifying the stability of the complex core. The isotopic distribution patterns of both these two peaks could be simulated [Figure IV-6a].

IR spectroscopy

The IR spectra (KBr pellet) of **1**and **2** are shown in Figure IV-8 and IV-9 respectively along with assignments for the latter. IR spectra of the ancillary ligands 1, 2- diaminoethane (en) and imidazole (Im) are shown in Figure IV-10 and Figure IV-11 respectively. Some of the broad IR bands of the free pterin ligand (H_2L, Scheme IV-1, Figure III-6) around 3131 cm^{-1}, 1684 cm^{-1} and 1382 – 1254 cm^{-1} are modified on complex formation due to deprotonation of the –COOH(6) and NH(3) groups. For both complexes **1** and **2,** the ν_{as} and ν_s vibrations of the $-CO_2'$(6) group appear around 1597 – 1590 cm^{-1} and 1326 cm^{-1} respectively; the Δ values ($\nu_{as} - \nu_s$ = 263 -271 cm^{-1}), are well within the range for monodentate carboxylate coordination.[87,88] The ν(C-O) mode of the pterin phenoxide(4) groups could be located around 1298 – 1305 cm^{-1} in these complexes. Tridentate pterin coordination involving the O(4), N(5) and CO_2'(6) functional

groups (Schemes IV-1 and IV-4) is indicated for both **1** and **2**. This is consistent with their x-ray structural data (Figures IV-1 and IV-2).

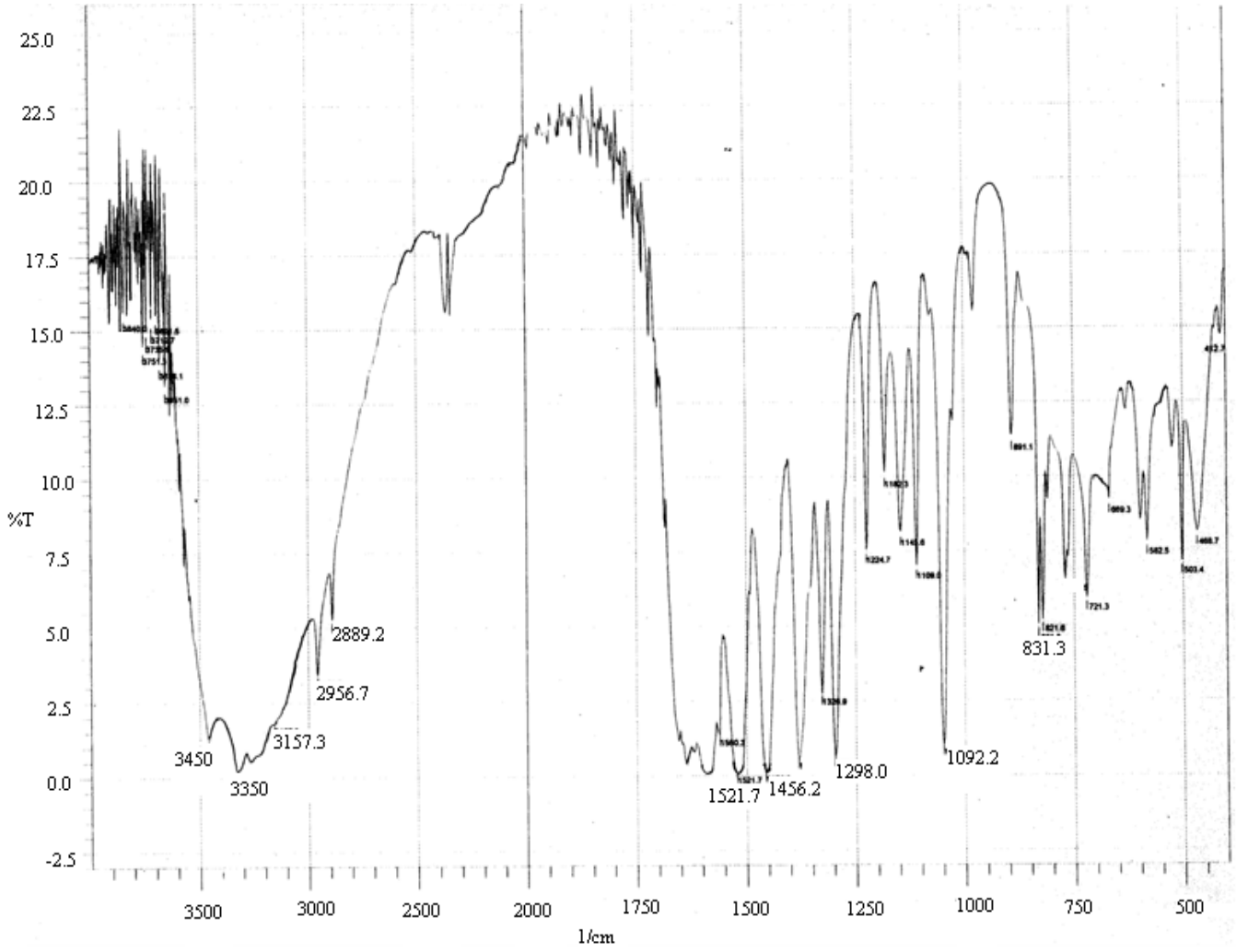

Figure IV-8. IR spectrum of **1** (KBr pellet)

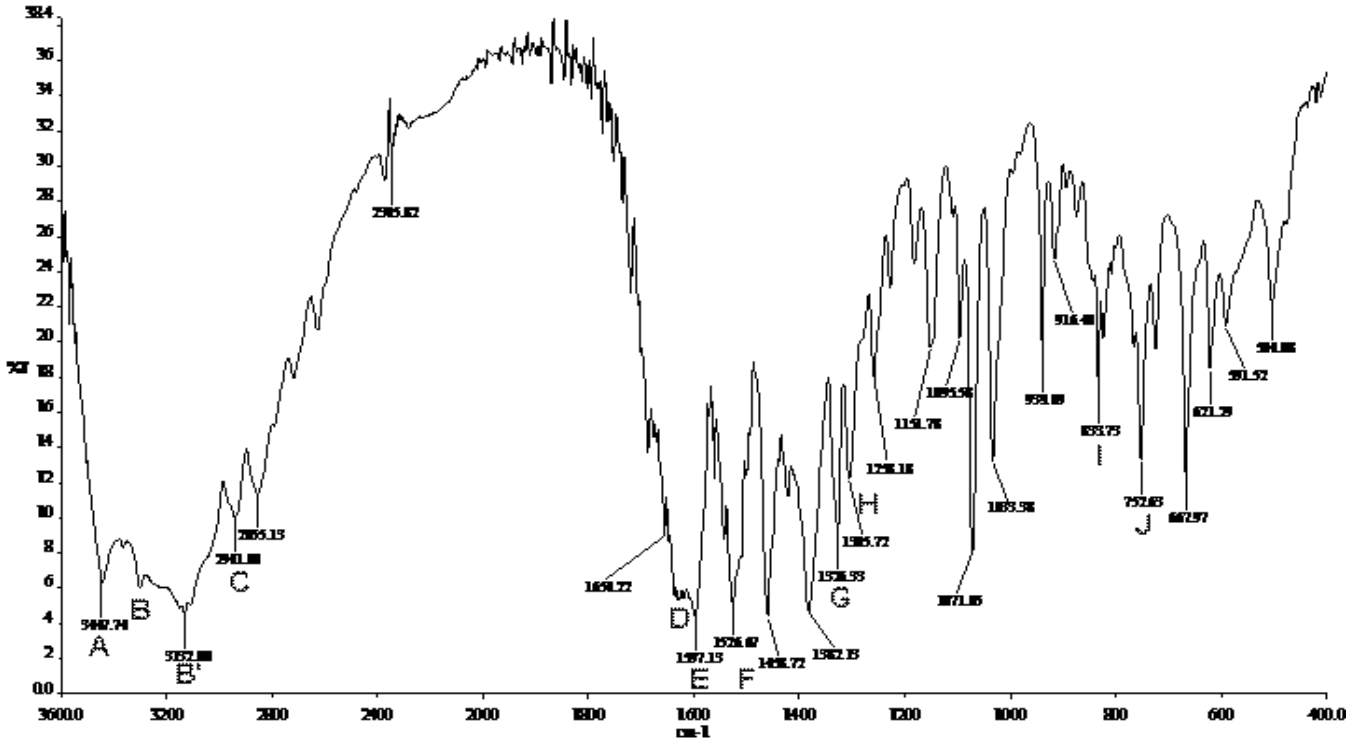

Figure IV-9. IR spectrum of compound **2** (KBr pellet)

A: Hydrogen bonded ν(OH) vibration;

B,B′: ν(NH) vibration of NH_2(2) of pterin and ‘en’ ligands;

C: ν(CH) vibrations;

D,F: ν(C=C) and ν(C=N) vibrations;

E: $\nu_{as}(CO_2')$, (N – H) bending vibrations;

G: $\nu_s(CO_2')$;

H: ν(C – O) of pterin phenoxide(4) group;

I,J: out- of- plane C – H bending vibration.

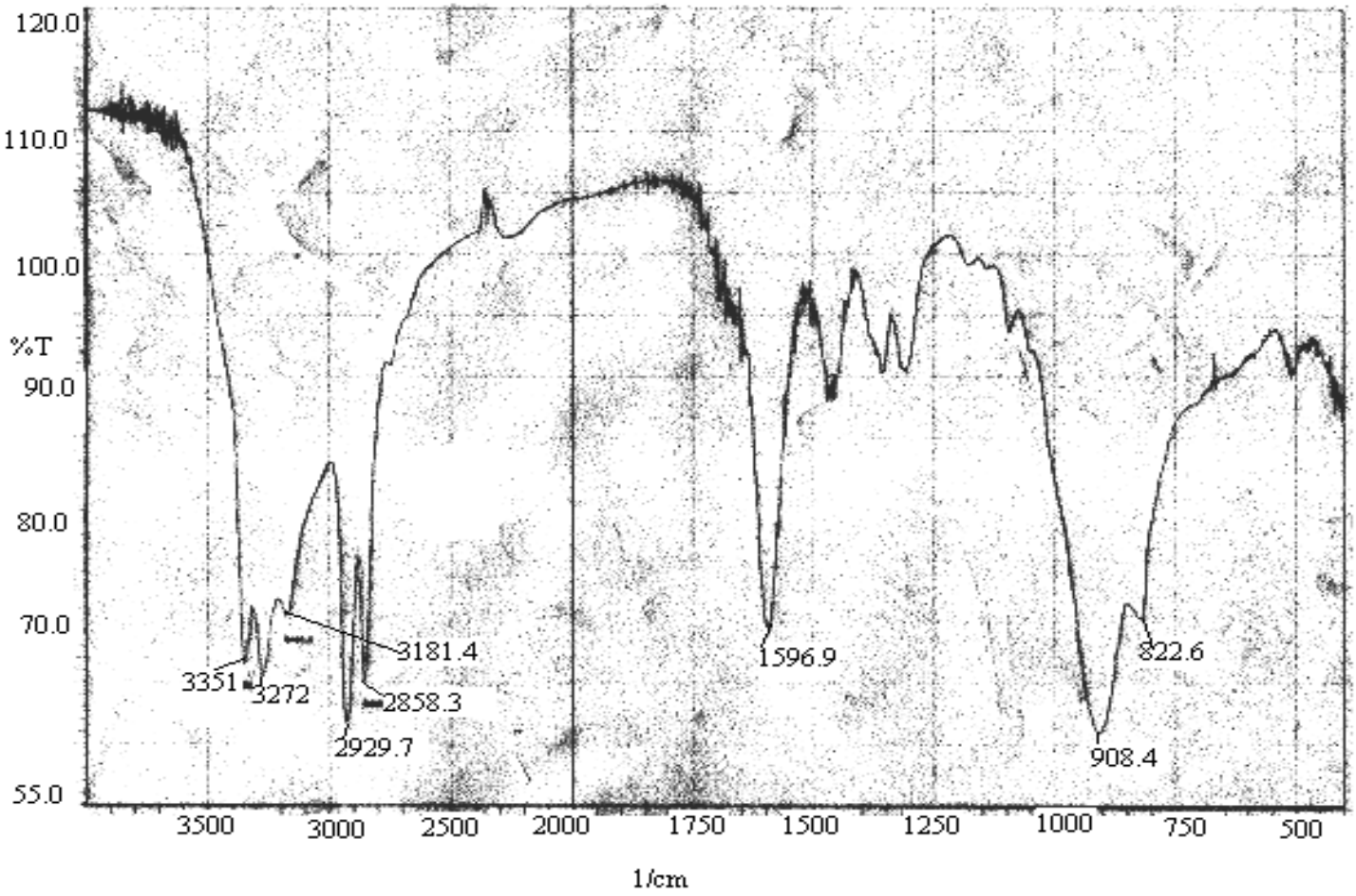

Figure IV-10. IR spectrum of 1, 2-diaminoethane (en)

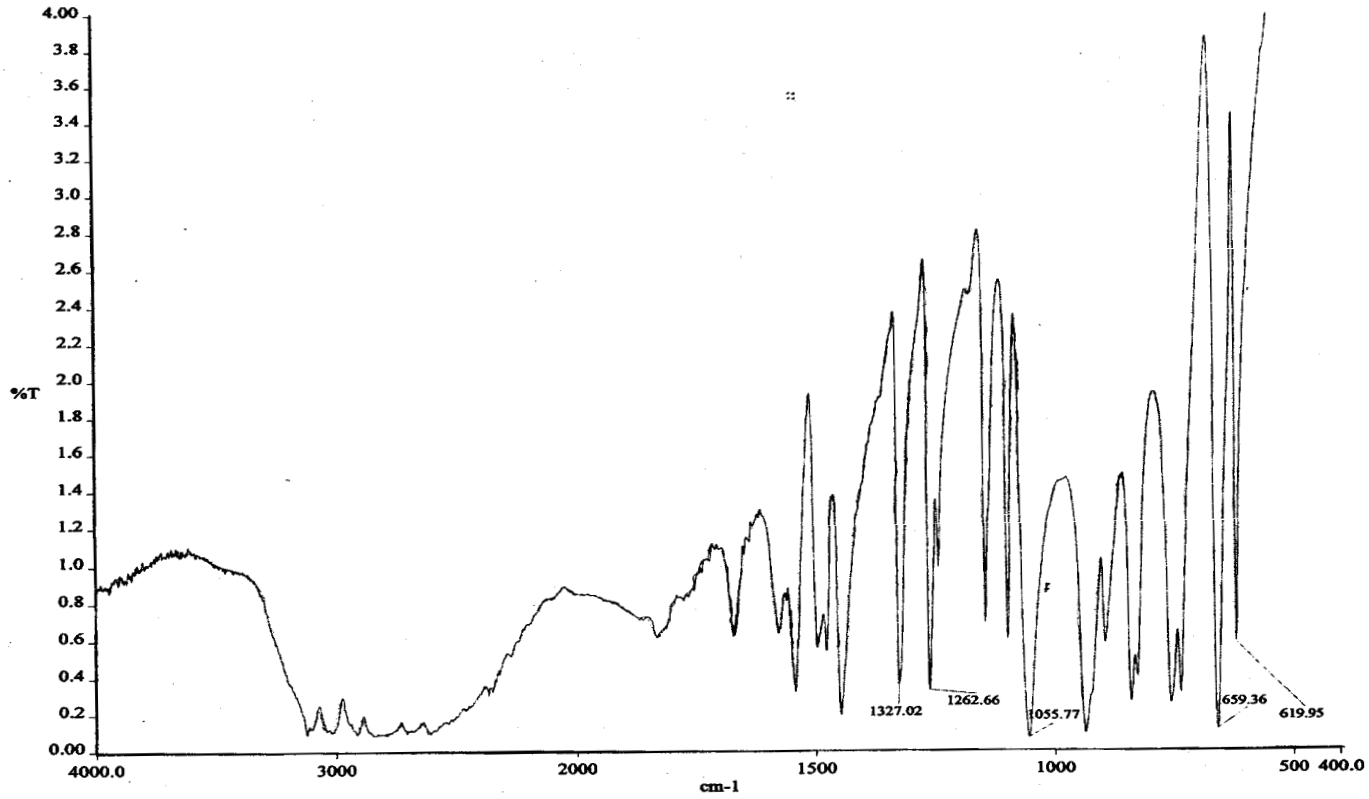

Figure IV-11. Spectrum of imidazole (Im) (KBr pellet)

UV-VIS spectroscopy

Table IV-7. Electronic spectral data of **1** in H_2O and **2** in CH_3OH

Sl. No.	Compound	λ_{max} nm (logε)
1.	**1**	258sh(3.97), 270(4.09), 341sh(3.51), 370(3.75), 401sh(3.41), 408sh(3.21), 946sh(2.74), 1004sh(2.745), 1057sh(2.76)
2.	**2**	270(4.26), 369(3.88), 542br(1.12), 620br(0.96), 698(1.21), 748(1.24), 812(1.43), 921br(0.88), 1063sh(1.32)

Electronic spectra (H_2O) of **1** and (CH_3OH) **2** are shown in Figure IV-12 and IV-13 respectively with Table IV-7 summarizing their essential features. Both of these two spectra are dominated by two intense bands at 270 nm and 369 – 370 nm, assignable to ligand $\pi \rightarrow \pi^*$ and LMCT bands respectively. Besides these, at high resolution a few broad, longer wavelength bands of lower intensity could be identified; they are usually associated with vibronic fine structures. Such spectral features may be elucidated in the light of energy level diagram of the Ni(II) d^8 system and symmetry considerations. Scheme IV-7 shows the partial Orgel diagram diagram of the d^8 system in an octahedral environment along with two specific examples including their band assignments.[90] Splitting of the middle

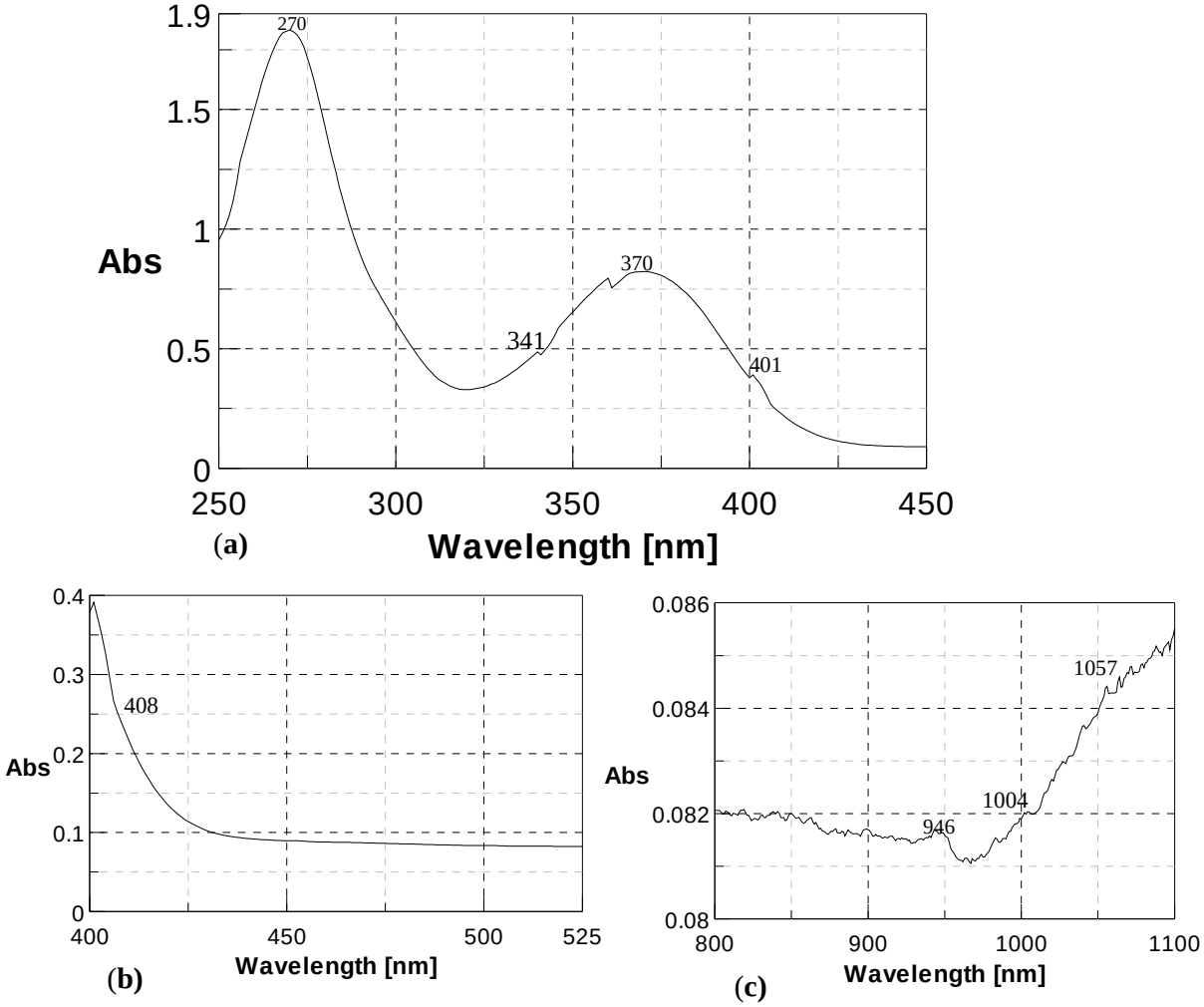

Figure IV-12. Electronic spectra of **1** in H_2O (1.48 x 10^{-4} mol dm^{-3})

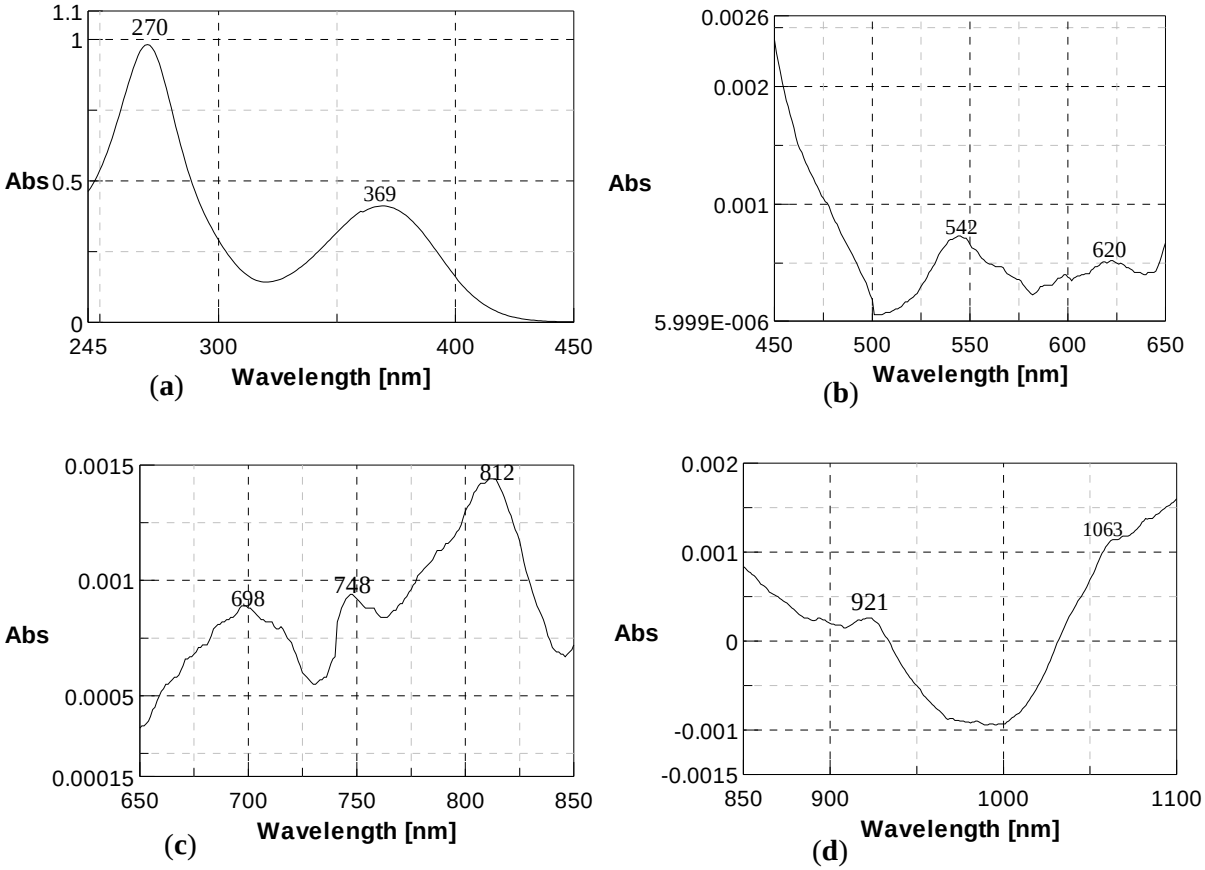

Figure IV-13. Electronic spectra of **2** in CH_3OH

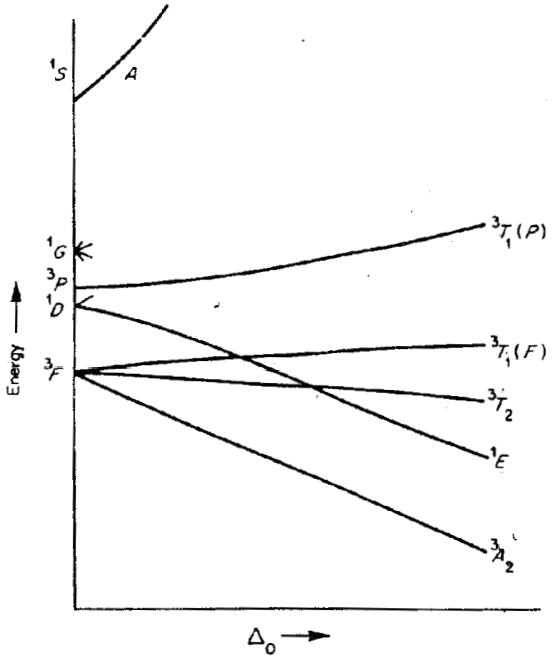

Partial energy-level diagram for a d^8 ion in an octahedral field, showing the triplet states and only the lowest singlet state.

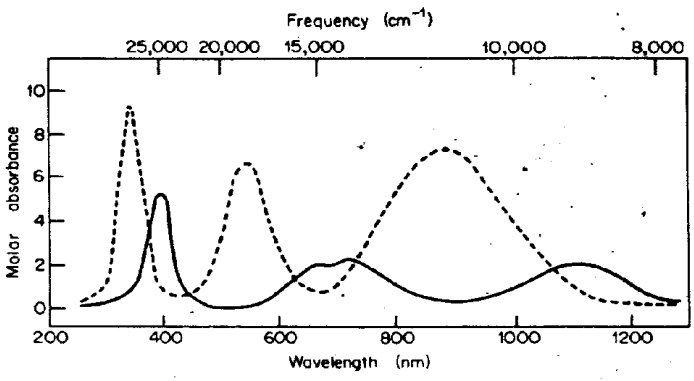

Absorption spectra of $[Ni(H_2O)_6]^{2+}$ (solid curve) and $[Ni(en)_3]^{2+}$ (dashed curve).

	Approximate band positions (cm^{-1})	
Transition	$[Ni(H_2O)_6]^{2+}$	$[Ni(en)_3]^{2+}$
$^3A_{2g} \rightarrow {}^3T_{2g}$	9,000	11,000
$^3A_{2g} \rightarrow {}^3T_{1g}(F)$	14,000	18,500
$^3A_{2g} \rightarrow {}^3T_{1g}(P)$	25,000	30,000

Scheme IV-7

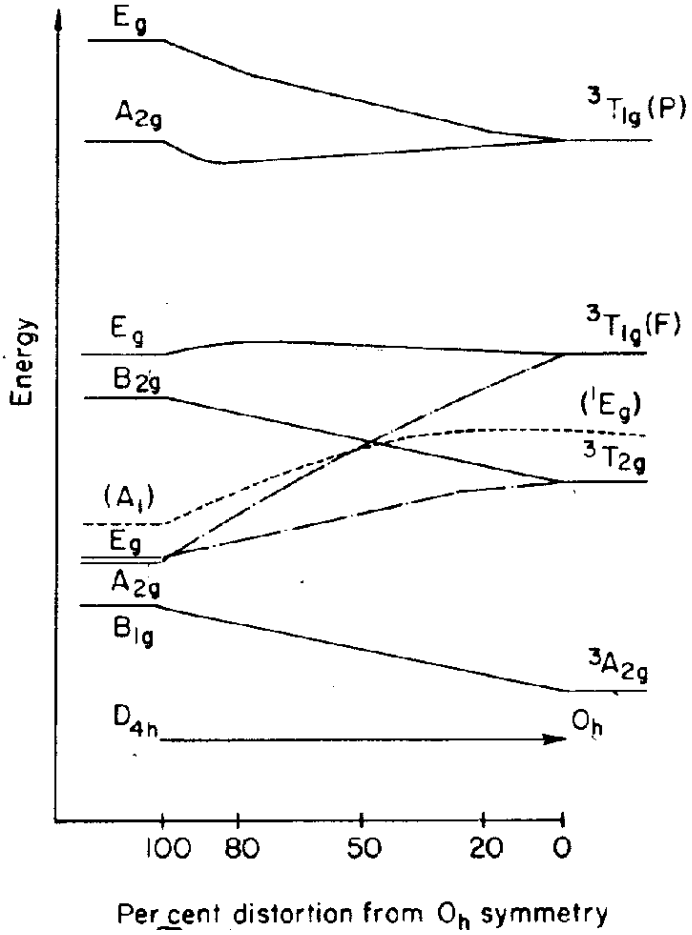

Scheme IV-8 Effects of tetragonal distortion on the energy levels of Ni(II). Reference: C. Furlani, and G. Sartori, *J. Inorg. Nucl. Chem.*, **8**, 126 (1958).

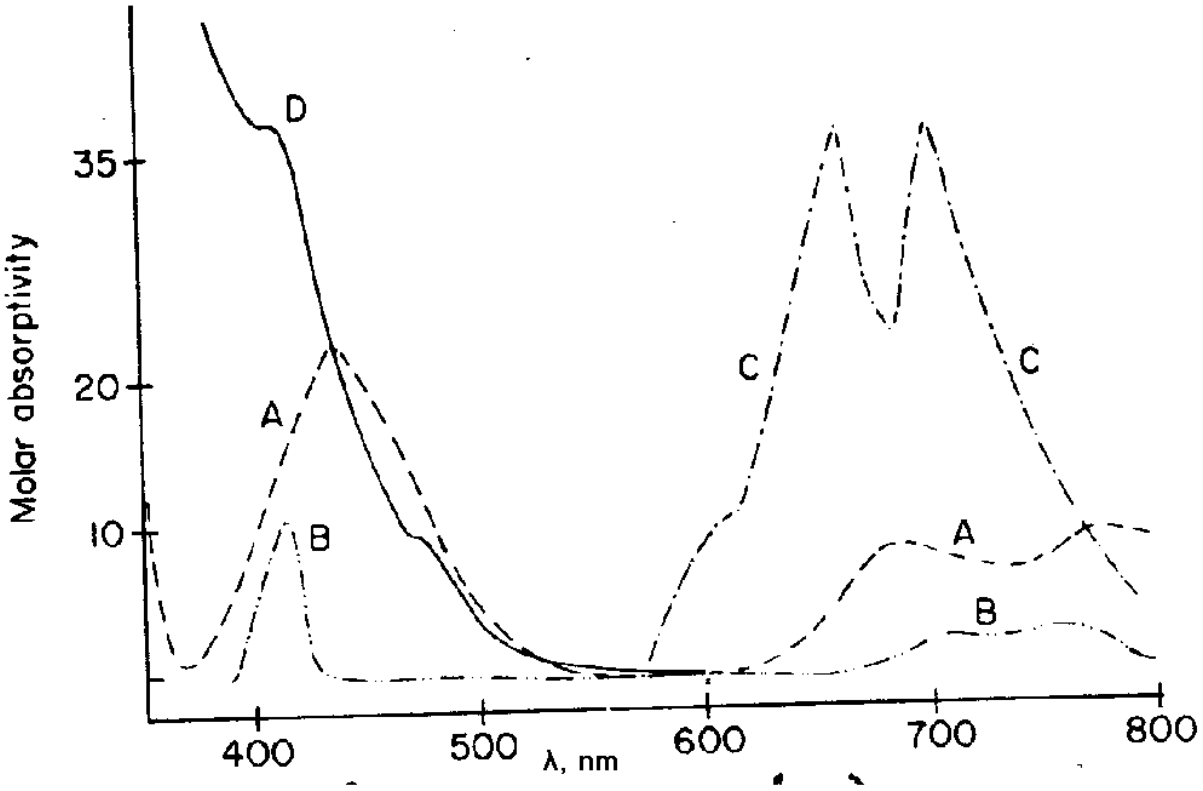

Scheme IV -9 Electronic absorption spectra of some nickel complexes. A. $Ni(\Phi_3PO)_4(ClO_4)_2$ in $CH_3NO_2(D_{2d})$; B, $Ni[(CH_3)_2SO]_6(ClO_4)_2$ in $(CH_3)_2SO(O_h)$; C, $NiCl_4^{2-}$ in $CH_3NO_2(T_d)$; D, Ni(II)(dimethylglyoxinate)$_2$ in $CHCl_3(D_{4h})$. Curve C is a plot of ε/5.

---

band in the $[Ni(H_2O)]^{2+}$ spectrum is due to spin –orbit coupling which mixes the $^3T_{1g}(F)$ and ^1E_g states which are quite close in energy at the Δ_0 value provided by $6H_2O$, while in the stronger crystal field of the 3en they are far apart so that no significant mixing occurs. Scheme IV-8 shows the effect of lowering of symmetry from $O_h \rightarrow D_{4h}$ on the electronic energy levels of the d^8 system. [89] As evident from the x-ray structural data of both **1** and **2**, there is considerable

departure from regular octahedral geometry associated with additional splitting of the energy levels, some of them being even raised in energy (Scheme IV-8). The more numerous signals in the LMCT region[325 – 425 nm; Figure IV-12(b) and Figure IV-13(b)] of **1,** may be ascribed to its lower symmetry as compared to that of **2**. Scheme IV-9 illustrates the effect of changes in symmetry on the electronic spectra of Ni(II) complexes; for a square planar complex (D_{4h}), there is little absorption in the longer wavelength region (600 – 800 nm).[89] In the light of Scheme IV-7 to IV-9 the broad, longer wavelength bands for **1** and **2** are assigned to spin-allowed as well as spin-forbidden 'd-d' transitions with considerable intensity stealing from the LMCT band (369 – 370 nm).[31]

Circular dichrosim spectroscopy

Figure IV-14 shows the CD spectra of **1** and **2** in H_2O indicating their low symmetry environments. Both signs and magnitudes of the associated cotton effects need attention. The negative Cotton effects around 370-384 nm may be assigned to LMCT transition. For **1** [Figure IV-14(a)] three positive Cotton effects could be identified at 487 nm, 684 nm and 762 nm respectively. In case of **2** [Figure IV-14(b)] such Cotton effects are observed at 445 nm, 549 nm and 775 nm, respectively. But the magnitudes of the Cotton effects are larger for **1** as compared to those of **2**. This is due to greater distortion from regular octahedral geometry for **1**. The δ-conformation of the 'en' chelate ring as observed from x-ray structural data, most likely decides the sign of the Cotton effects around 400-850 nm which correspond to some of the electronic transitions enlisted in Table IV-7.

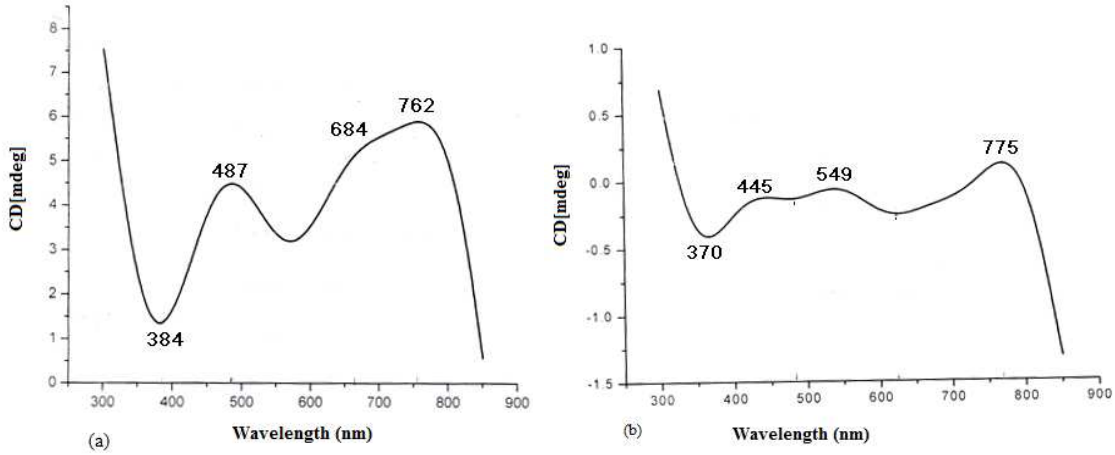

Figure IV-14. CD spectra in H_2O: (a) **1** (2.55 x10^{-3} M); (b) **2** (2.26 x 10^{-3}M).

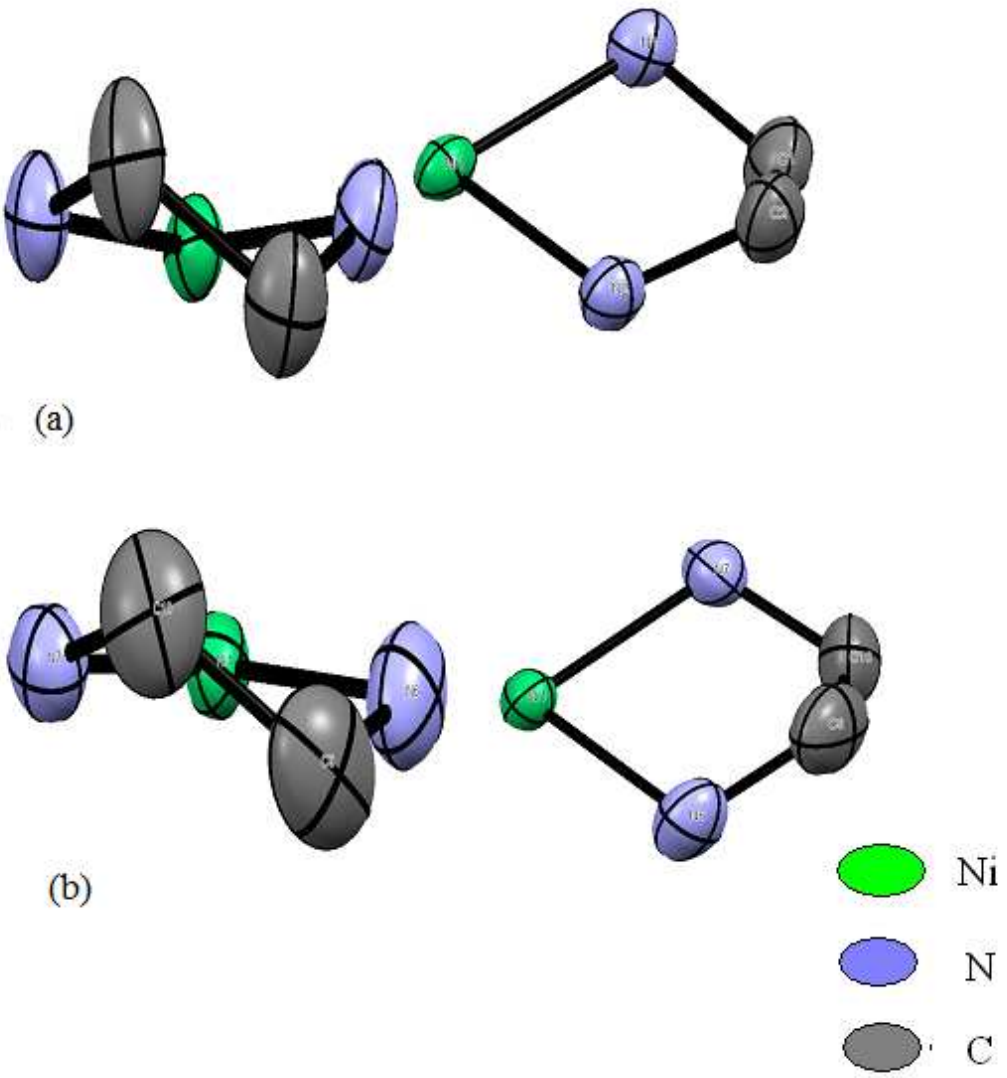

Figure IV-15. δ – conformation of the ethelenediamine chelate ring for (a) **1**and (b) **2**, as obtained from their x-ray structural data; other donor atoms [Figure IV-1 and IV-2] are omitted for enhancing the effect chelate ring puckering.

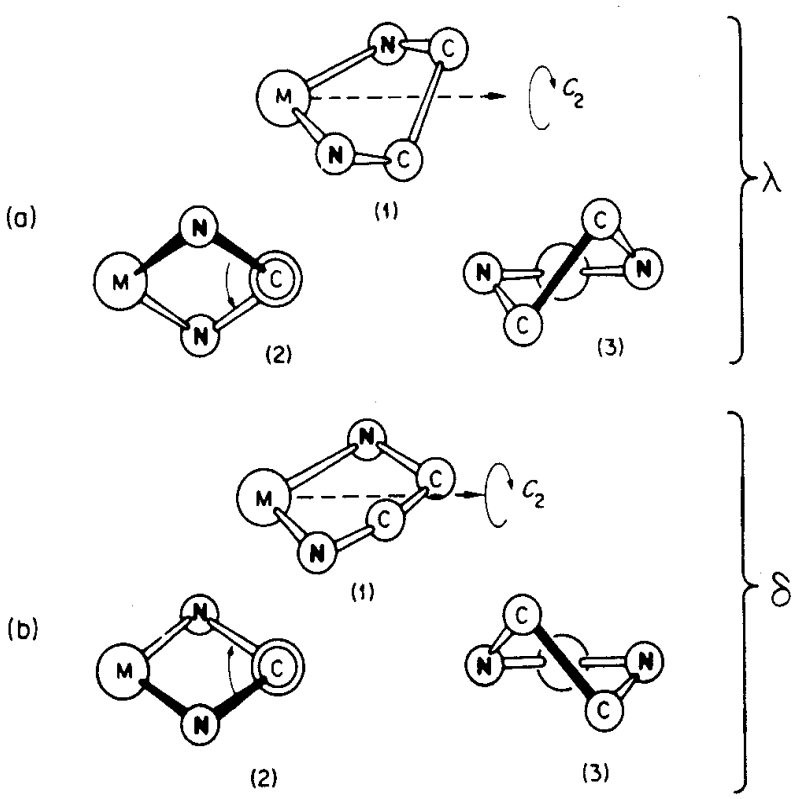

Scheme IV-10 Different way of viewing the puckering of ethylenediamine chelate rings. The absolute configurations λ and δ are defined.[79]

Scheme IV-10 shows the λ-/δ- puckering of ethylene diamine (en) chelate ring. Projections of the x-ray structural data of **1** and **2** for viewing the puckering of the 'en' chelate ring in each case, are shown in Figure IV-15. A comparison with Scheme IV-10 indicates δ-conformation of the 'en' ring in each case. Now the most important inference of this chiroptical study is that steric repulsion of the two chelate rings associated with the pterin ligand residue (L^{2-}) could be minimised only for the δ-conformation, as above.

Fluorescence Emission Sprctra

The fluorescence emission spectra (CH_3OH) of **1**, **1R**, **2**, and **2R** are shown in Figure IV-16 and IV-17 respectively. In all these cases the emission maximum appears at 450 nm. For the pterin ligand (in aqueous NaOH solution) such emission maximum appears (Figure II-11) at 449 nm. It is apparent that on mixed ligand complex formation in **1** and **2**, there is considerable drop in fluorescence intensity, with the emission maximum position remaining essentially unchanged. Apparently there is some pathway through which the vibronic energy can dissipate, associated with this drop in fluorescence intensity. Again, the enhance fluroscence intensity of the $NaBH_4$ reduced compounds (**1R** and **2R**) can be correlated with the greater electronic circulation in the 7, 8- dihydro form of the pterin ligand residue. (L'^{2-} ; Scheme IV-6). Existence of the 7, 8-dihydro form in **1R** and **2R** could be inferred from the ^1H NMR spectral data of a Cu(I) complex in chapter II. Most organic fluorescence molecules contain conjugated system of double bonds with extended π orbitals in a planer cyclic/rigid structure and not many loosely coupled substituent's through which the electronic energy can dissipate. Even the pH dependence fluorescence property is interesting, e.g. no fluorescence is observed for the protonated form of biopterin but the anion is strongly fluorescent.[35-37]

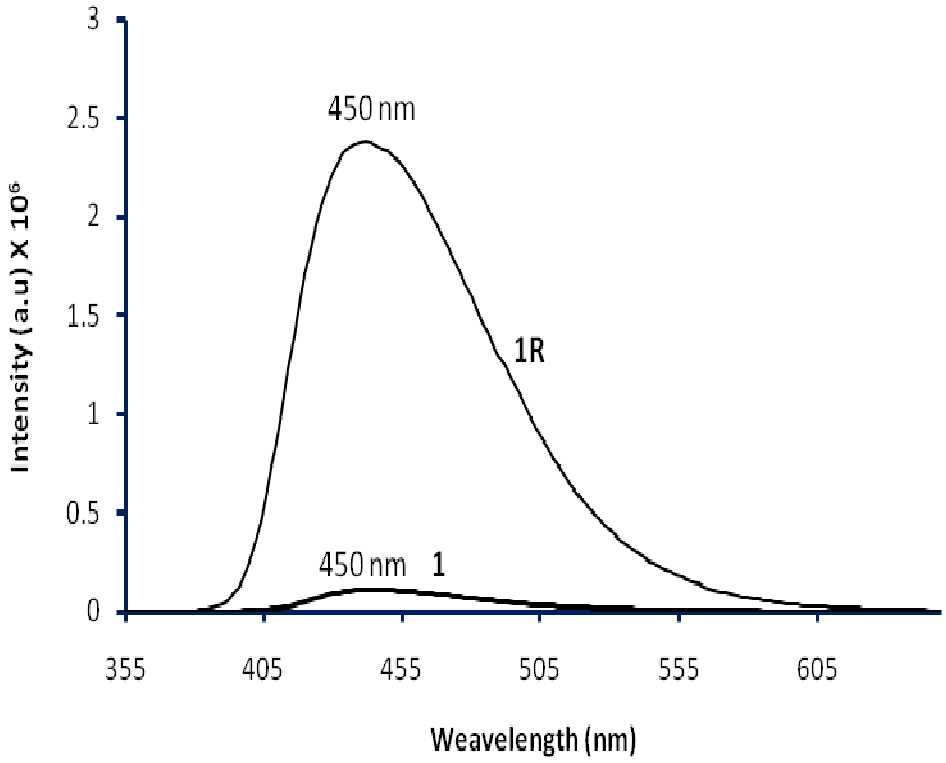

Figure IV-16. Fluorescence emission spectra of **1**(CH_3OH, 1.4 x 10^{-4} M), **1R** (CH_3OH, 1.4x10^{-4} M).

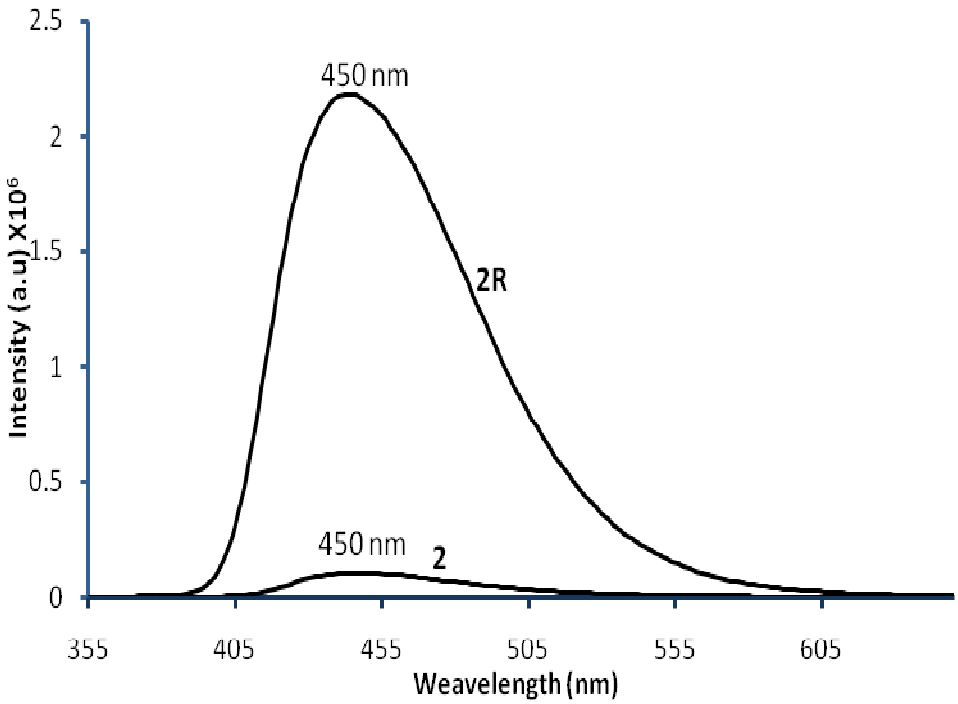

Figure IV-17. Fluorescence emission spectra of **2** (CH_3OH, 1.4 x 10^{-4} M), **2R** (CH_3OH, 1.4 x 10^{-4} M).

EPR spectroscopy and magnetic susceptibility data

Magnetic susceptibility data (μ_{eff}, 299K) of complexes **1** and **2** are 2.90 BM and 2.89 BM respectively. Both these values are close to the spin-only value (2.83 BM) for two unpaired electrons, with small orbital contribution. However, their EPR spectral data could not be recorded properly due to the problem of line broadening. For d^8 ion [e.g. Ni(II)] in distorted octahedral fields, the zero-field splitting becomes larger and EPR signals are quite difficult to observe. As an example, the EPR spectral response of **2** is shown in Figure IV-18 and it is inconclusive. Here the μ_{eff} values provide the necessary guide lines about electronic structures here.

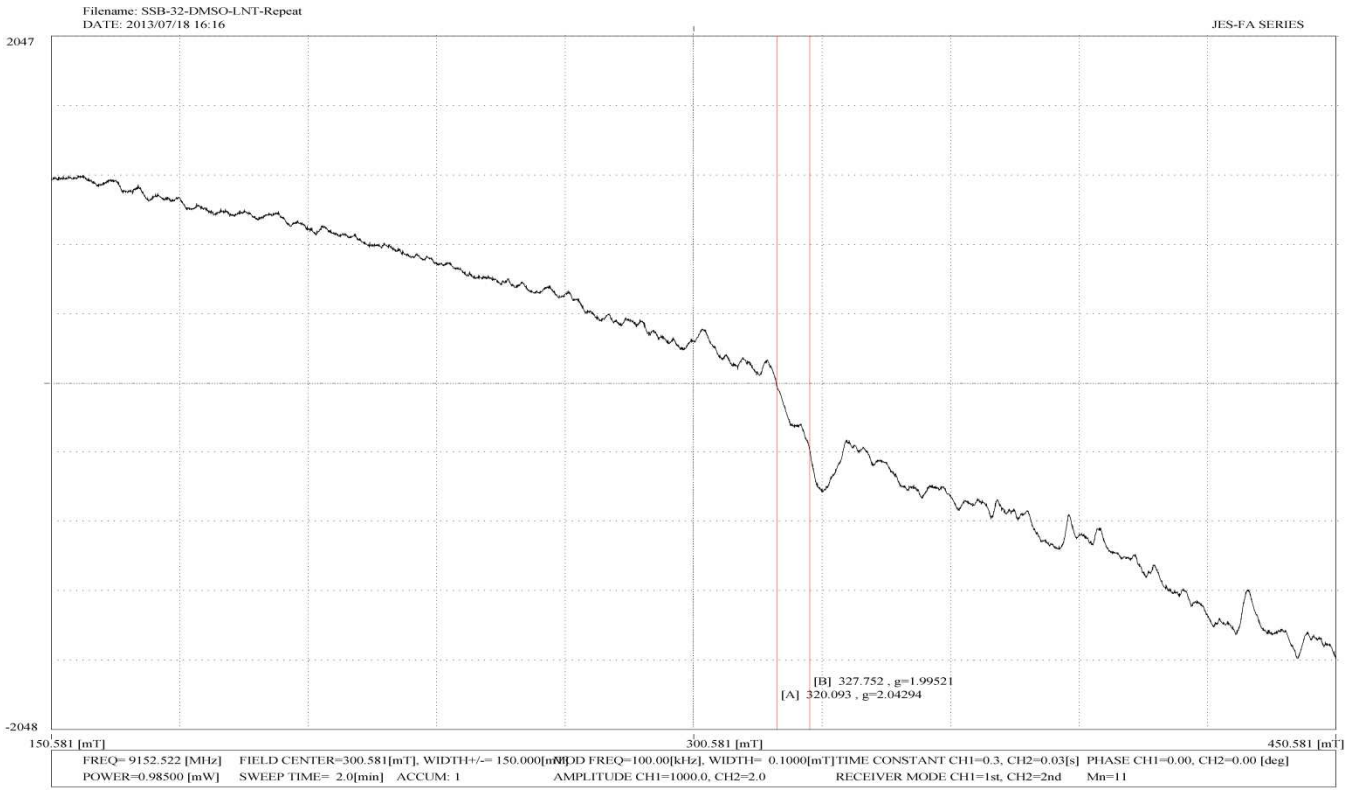

Figure IV-18. X-band EPR spectrum of **2** in DMSO at 77K.

Cyclic voltammetry

Figure IV-19 shows the cyclic voltammetry data of **2** in DMSO. A metal-centred reduction occurs at -0.744 V; the corresponding re oxidation peak could be located at -0.669 V. The ΔE_p value (75 mV) indicates the quasi-reversible nature of this redox process; besides this, a ligand reduction peak occurs at – 1.651 V. Here the quasi-reversible process can be assigned as follows –

$$Ni(II) + e \rightleftharpoons Ni(I)$$

This facile change over between the two oxidation states of nickel can be justified in terms of the relevant Frost diagram (Scheme IV-11). It is evident that the change over between the +1 and +2 oxidation states of nickel can be achieved with small change in free energy ($\Delta G^\circ = -nFE^\circ$). Significance of this information obtained in the time scale of cyclic voltammetry , is further clarified during the reactivity study with $NaBH_4$ (shown later) as well as isolation of a dark coloured compound (**2R**) through $NaBH_4$ reduction where both the metal and pterin ligand centers are in the reduced forms [Ni(I) and 7, 8-dihydro state of pterin].

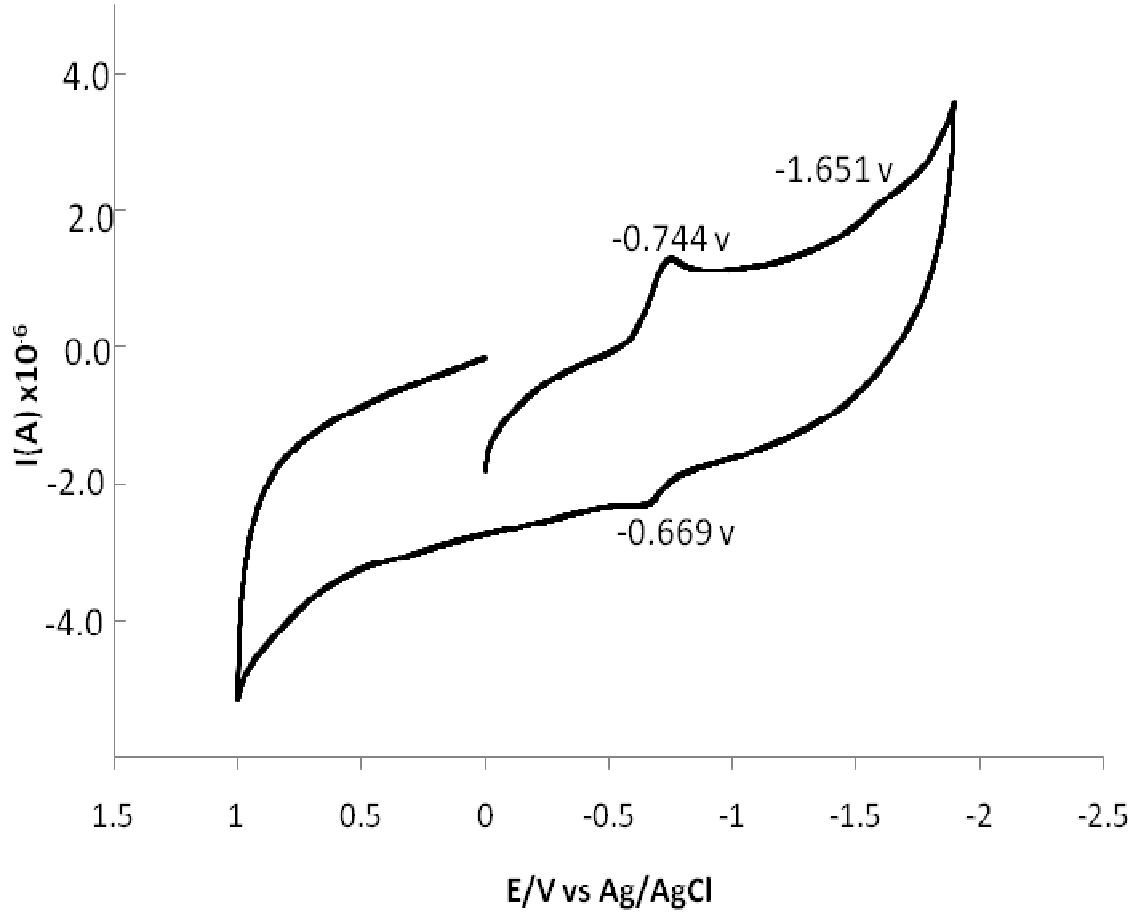

Figure IV-19. Cyclic voltammogram of **2** in DMSO (0.1 mM, 0.1M TBAP, GCE, 100 mVs^{-1})

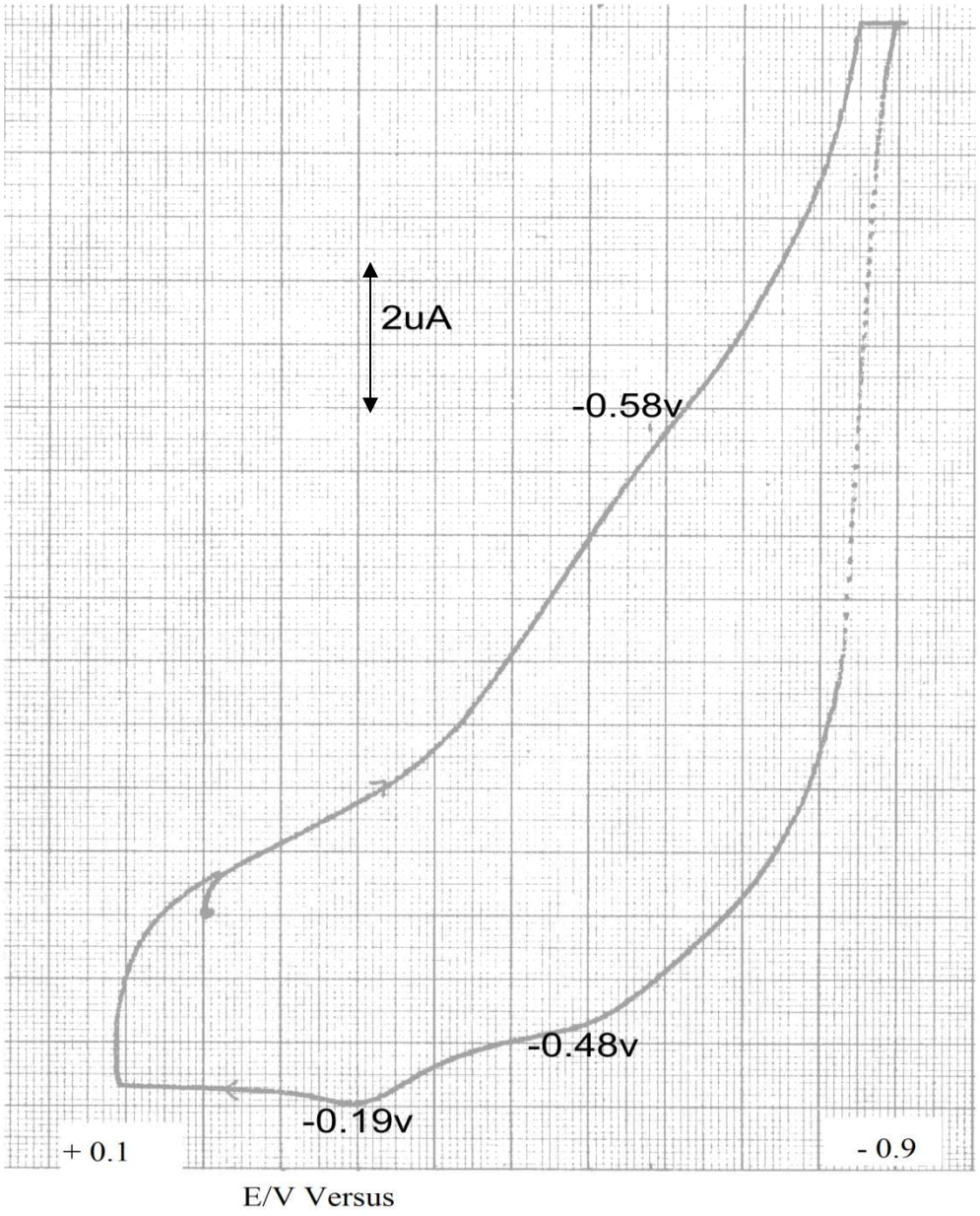

Figure IV-20. Cyclic voltammogram of **1** in H_2O (1 mM, 0.1 M KNO_3, GCE, 250 mVs^{-1})

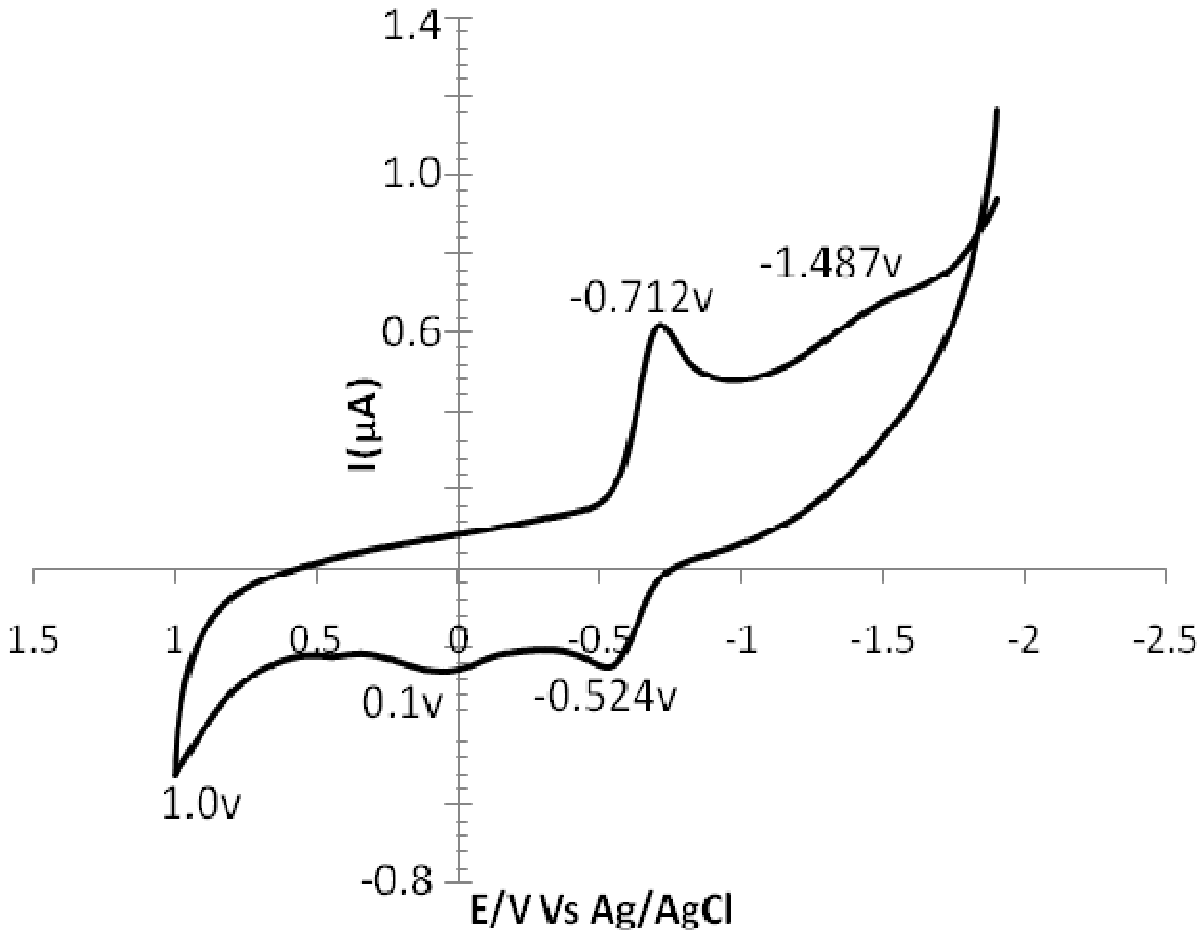

Figure IV -21. Cyclic voltammetry data of **1** in DMSO (1mM, 0.1M TBAP, GCE, 100 mVs^{-1})

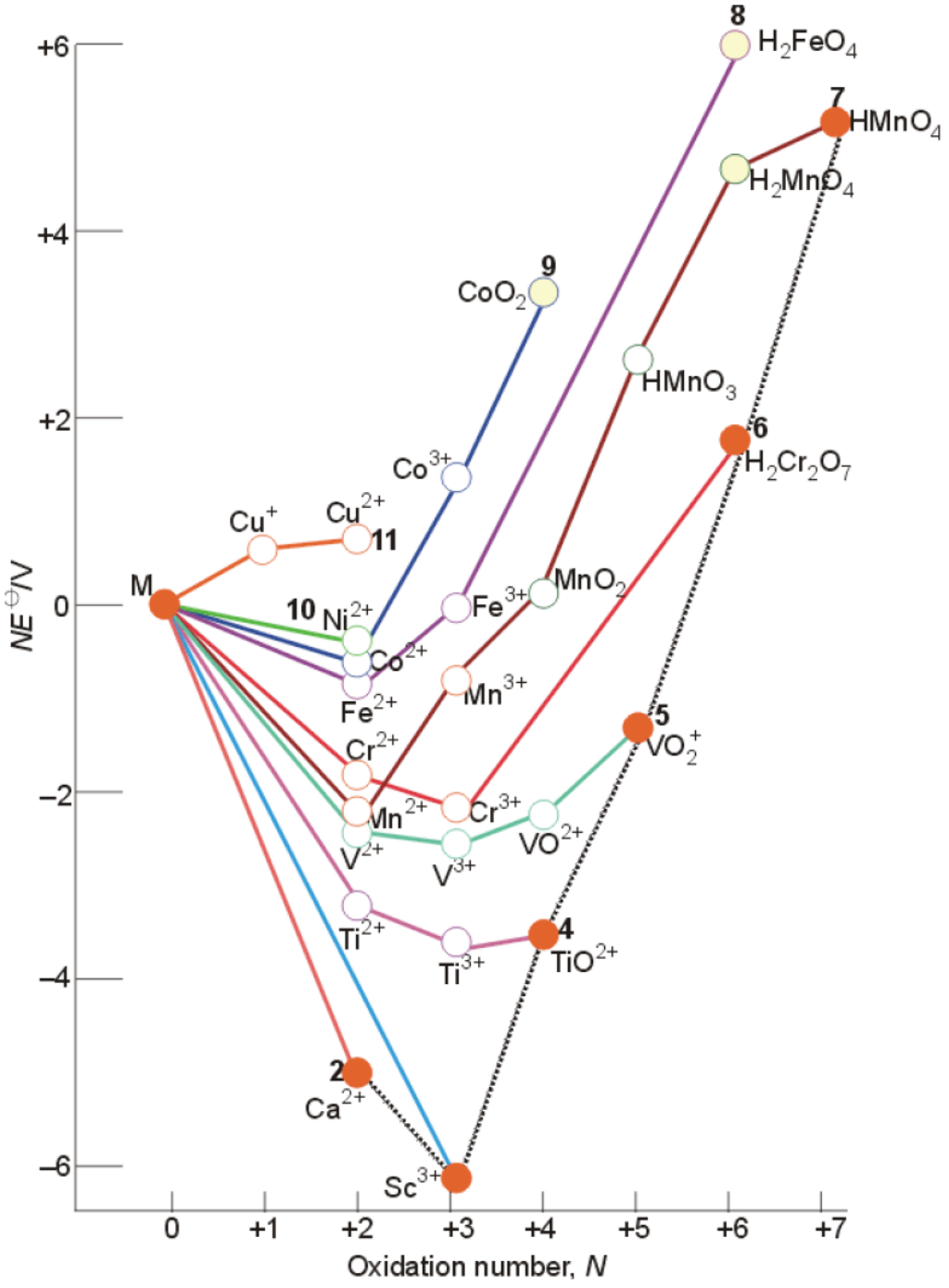

Scheme IV-11 Frost diagram of the first transition series in acidic solution (pH = 0)[91]

Elucidation of these metal-and pterin-centred reductions is provided later in the light of Frontier orbital energies (DFT).

Cyclic voltammetry data of **1** in H_2O is shown in Figure IV-20. Here the metal-centred reduction process [Ni(II) → Ni(I)] could be located at – 0.58 V; the reduction product is quite unstable in aqueous medium, leading to essentially irreversible behavior. Two reoxidation peaks appear at -0.48 V and -0.19 V respectively.

Cyclic voltammetry data of **1** in DMSO is depicted in Figure IV-21. The metal-centred reduction and reoxidation peaks appear at -0.712 V and -0.524 V respectively (ΔE_p = 188 mV). Obviously, in DMSO the reduced species has a longer life time as compared to that in H_2O. A ligand reduction peak appears at -1.487 V.

Reactivity of 1 towards imidazole

1 possesses an aquo group [Figure IV-1] and provides with an opportunity for exploring its group substitution reaction using imidazole (Im) as the reagent. The ubiquitous nature of the histidine residue in metallobiomolecules, makes this study all the more significant as imidazole is a model of histidine. Kinetics of the following reaction is presented here:

$[Ni(L)(en)(H_2O)].2H_2O + Im \rightarrow [Ni(L)(en)(Im)]. 2H_2O + H_2O$

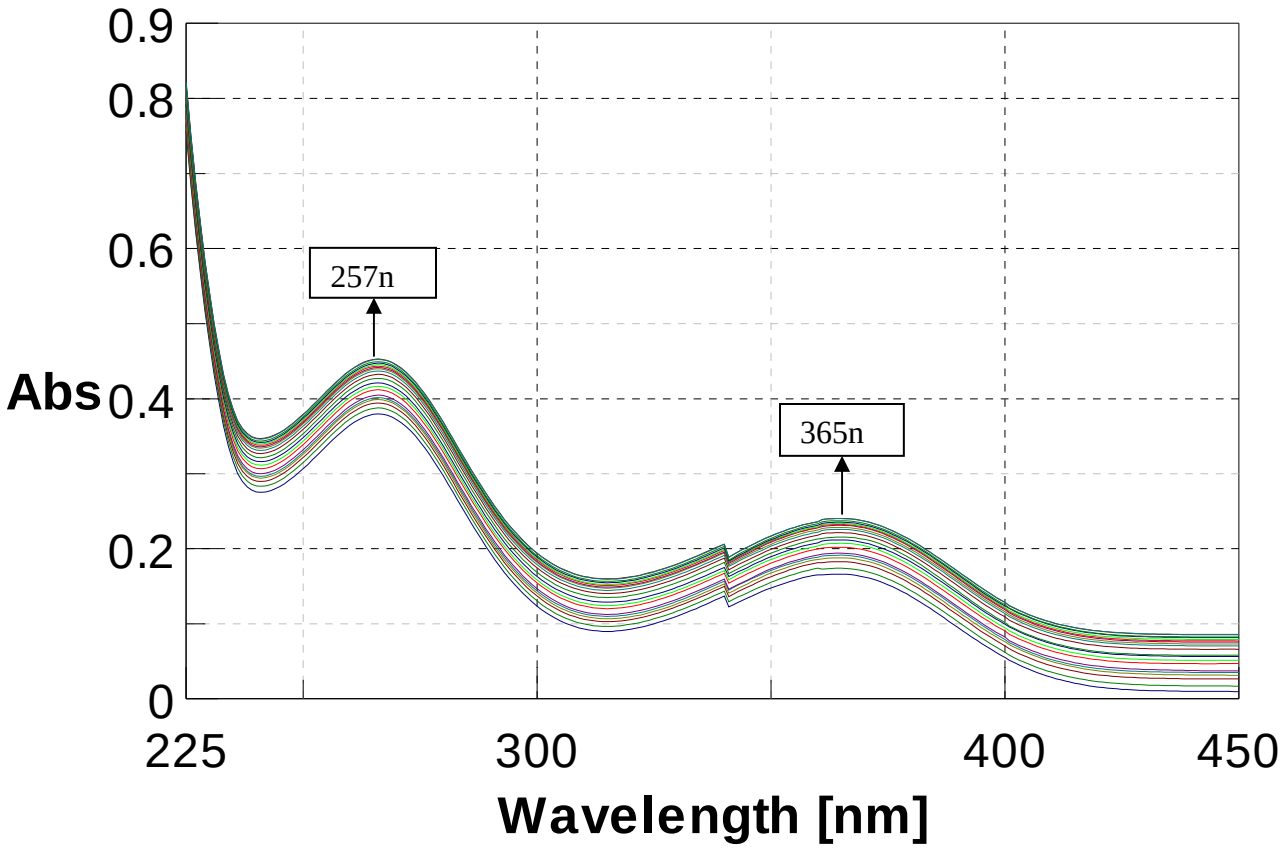

Figure IV-22. Absorption spectral changes recorded at 2 min interval during the reaction of (**1**) ($5.8x10^{-5}$M) with imidazole (Im) ($4.8x10^{-3}$M) in CH_3OH at 311K. The break at 340 nm in the spectral curve is due to lamp change over inside the instrument.

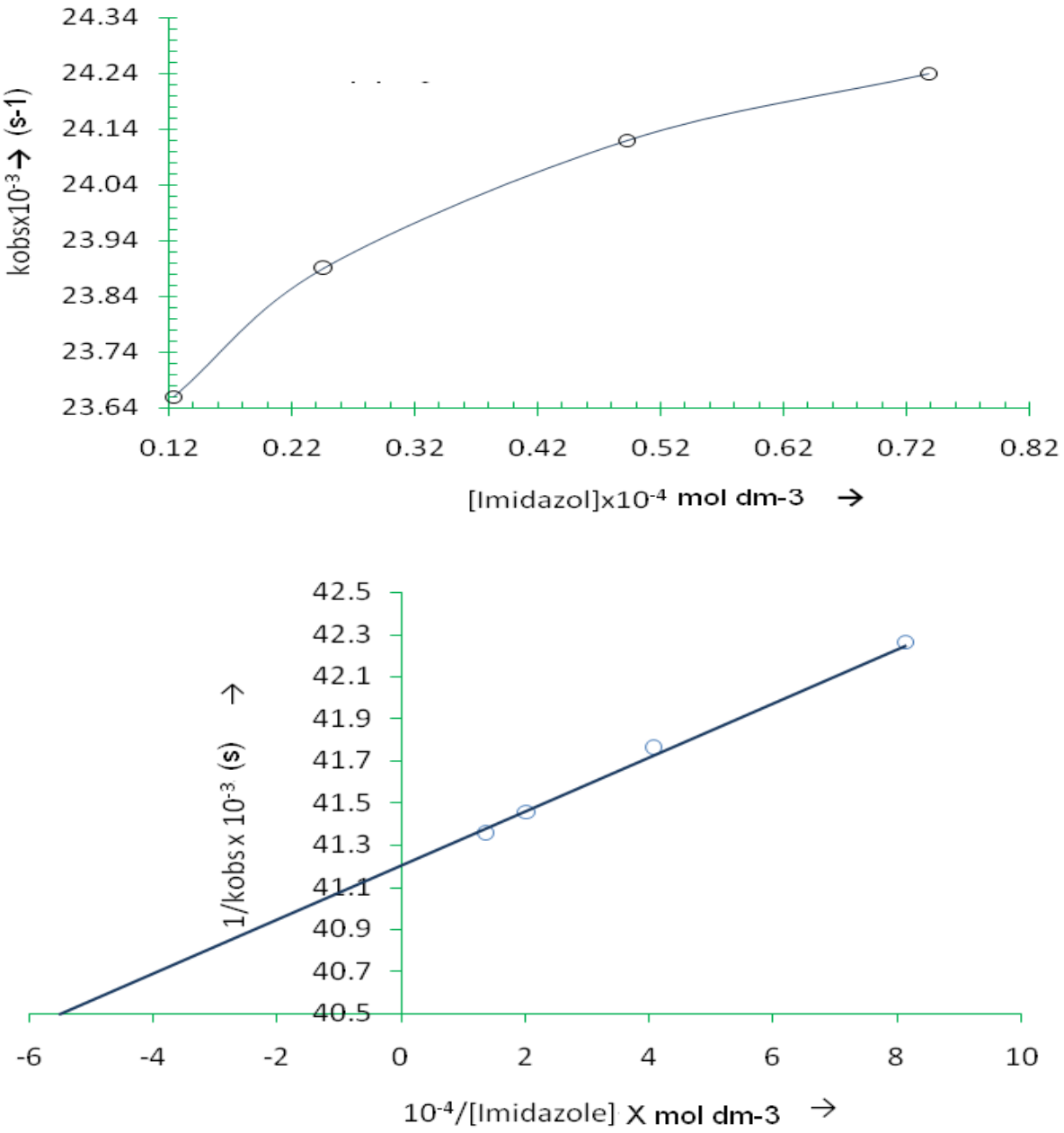

Figure IV-23. (a)Dependence of the rate of reaction of (**1**) (5.8×10^{-5}M) with 20-100 times Im in CH_3OH at 334K on Im; (b) the corresponding double reciprocal plot.

Stoichiometry of the above reaction has been established x-ray structurally (Figure IV-2), for characterizing the imidazole substituted product **2**. For obtaining a reasonable reaction rate, a

higher temperature range (308 – 328K) has been utilize here.Figure IV-22 represents the absorption spectral changes during the reaction of **1** with imidazloe in CH_3OH. Kinetics of this reaction was followed at 365 nm under psudo first order conditions (using ca. 20-100 times excess of imidazole) and four different temperatures (range 308 – 328K). From the Eyring plot the entropy of activation $\Delta S^{\neq}$ was found to be -178.5 J mol^{-1} deg^{-1}; the negative $\Delta S^{\neq}$ value indicates the associative nature of this substitution process. Absence of any isosbestic point in the overlay scans, suggests that the reactant aquo complex **1** is not converted directly into the imdazole substituted product **2**, but an intermediate step is involved. The negative $\Delta S^{\neq}$ value points towards the formation of a 7-coordinated intermediate with imidazole, which is ultimately converted to **2** along with the loss of the aquo group.

Observed rate constants were determined by least square method from the plots of $\log(A_\infty - A_t)$, versus time, which were linear for almost 3 half-lifes.[92] The average k_{obs} value of 2.4×10^{-2} s^{-1} is consistent with a group substitution process.[92,97,98] Figure IV-23(a) shows the plot of observed rate constant (k_{obs}, sec^{-1}) versus [Imidazole]. The reaction system exhibits saturation kinetics at high substrate (Im) concentration, indicating applicability of Scheme IV – 12.

$$\mathbf{(1)} + \mathrm{Im} \underset{k_{-1}}{\overset{k_1}{\rightleftharpoons}} [\mathbf{(1)}(\mathrm{Im})] \overset{k_2}{\rightleftharpoons} \mathbf{(2)} + H_2O$$

Scheme IV-12

In terms of Scheme IV-12 the observed rate constant (k_{obs}) can be represented as follows,[93] where [S] represents the concentrations of the substrate (Im):

$$k_{obs} = (k_2[S]/K_m + [S]), \qquad (1)$$

where $K_m = (k_2 + k_{-1})/k_1$ or

$1/k_{obs} = 1/k_2 + K_m/k_2[S]$ (2)

Where S = Im

The plot of $1/k_{obs}$ versus [1/ Im] should give a straight line with $1/k_2$ as the intercept and K_m/k_2 as the slope. The x-axis intercept equals $1/K_m$. From the double reciprocal plot of $1/k_{obs}$ versus [1/ Im] [(Figure IV-23(b)], k_2 and K_m were calculated as 2.4×10^{-2} s^{-1} and 1.82×10^{-4} mol dm^{-3} respectively at 308 K.

Reactivity of 1 towards $NaBH_4$

Taking hints from the cyclic voltammetry data [Figure IV-21] of **1** as well as the Frost diagram of the Ni(I)/Ni(II) couple (Scheme IV-11), reactivity of **1** is explored towards a typical reducing agent like $NaBH_4$. $NaBH_4$ is quite useful in pterin chemistry for its ability to reduce the pyrazine part of the pterin ring.[22,23] This aspect is relevant to the dihydro and tetrahydro states of biopterin (Scheme IV-13: BH_2/BH_4), which is the essential cofactor for phenylalanine hydroxylase (PAH) type metalloenzymes.[7,8,52-55]

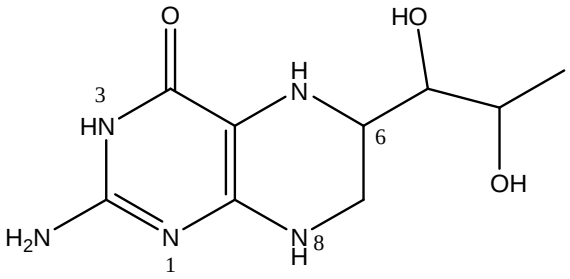

5, 6, 7, 8- tetrahydrobiopterin (BH_4)

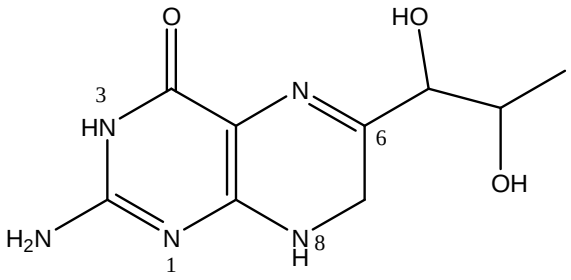

7, 8- dihydrobiopterin (BH_2)

Scheme IV-12

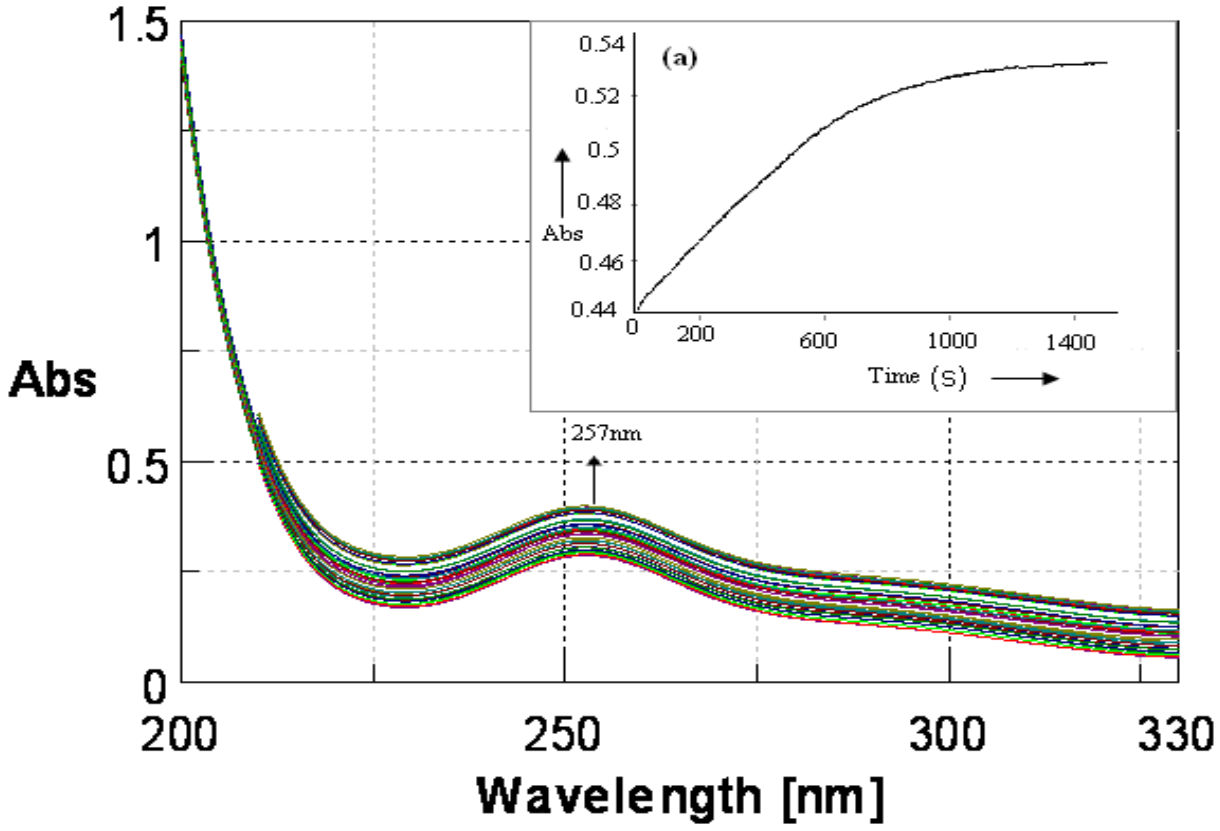

Figure IV-24. Absorption spectral changes recorded at 1.5 min interval during the reaction of **1** (5.8×10^{-5}M) with $NaBH_4$ (4.59×10^{-3}M) in CH_3OH; (a) absorption spectral changes recorded at 257 nm represent the absorbance versus time curve at 311K

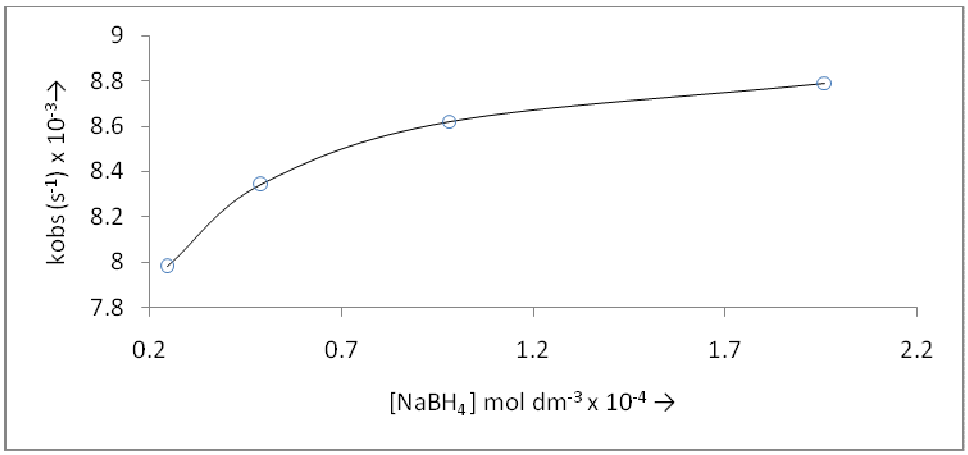

(a)

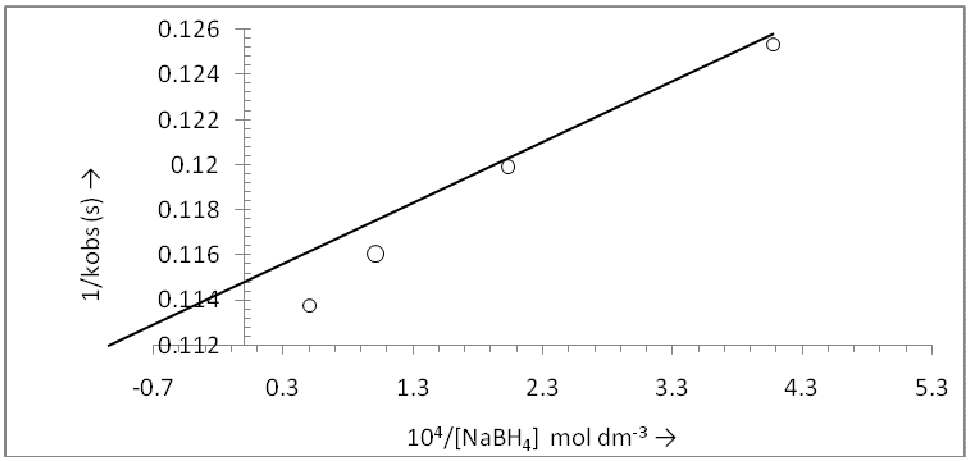

(b)

Figure IV-25. (a) Dependence of the rate of reaction of **1** (5.8×10^{-5}M) and 20-100 times of $NaBH_4$ in CH_3OH at 311K on $NaBH_4$; (b) the corresponding double reciprocal plot.

Thus we have the opportunity of exploring the metal-centered and pterin-centered redox reactvityes of **1** with $NaBH_4$. Figure IV-24 shows the relevant overlay scans, highlighting the reaction between **1** and $NaBH_4$ in CH_3OH. The reaction levels off after ca. 20 min. kinetics of this reaction was followed at 257 nm and four different temperatures (rang 300 -330K) under psudo-first order conditions (using 10 – 140 times excess of $NaBH_4$). From the plots of $\log(A_\infty$ -

A_t) versus time, which were linear for ca. 3 half-lives, k_{obs} values were obtained by least square method. An average k_{obs} value of 8.4 x 10^{-3} s^{-1} was found as well as an entropy of activation ($\Delta S^{\neq}$) parameter of – 198.5 J $mol^{-1}deg^{-1}$, respectively. The negative sign of the latter parameter indicates an overall associative pathway.

$$(\mathbf{1}) + NaBH_4 \underset{k_{-1}}{\overset{k_1}{\rightleftharpoons}} [(\mathbf{1})(NaBH_4)] \xrightarrow{k_2} \mathbf{1R} + \text{other product}$$

Scheme IV-13

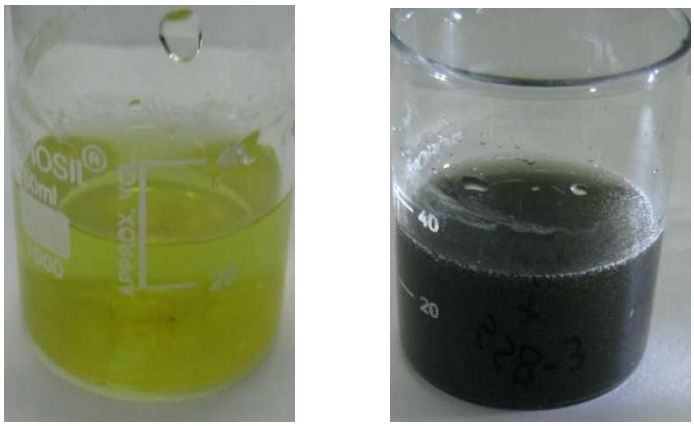

(a) (b)

Figure IV-26. (a) Colour of the Ni(II) complex **1**: it is dark brown in the solid state but is yellow-green in aquous solution;

(b) colour of the corresponding $NaBH_4$ reduced compound, **1R** which is dark coloured.

As evident from the Figure IV-25(a) the system exhibits substrate saturation kinetics at high substrate ($NaBH_4$) concentration, so that Scheme IV-13 may be applied. Now the observed rate constants (k_{obs}) can be represented as follows.[92,93]

$$k_{obs} = (k_2[S]/K_m + [S]), \qquad (3)$$

where $K_m = (k_2 + k_{-1})/k_1$ or

$$1/k_{obs} = 1/k_2 + K_m/k_2[S] \qquad (4)$$

where S = $NaBH_4$

The plot of $1/k_{obs}$ versus $[1/NaBH_4]$ should give a straight line with $1/k_2$ as the intercept and K_m/k_2 as the slope. The intercept on the x-axis gives $1/K_m$. Accordingly Figure IV-26(b) yields the following data:

$k_2 = 8.8 \times 10^{-3}\ s^{-1}$

$k_M = 1.4 \times 10^{-3}$ mol dm^{-3}.

The above experimental data may be assessed in the light of the following facts:

(1) Figure III-16 depicts the reactivity of the free pterin ligand towards $NaBH_4$, where the absorption spectral change behavior is quite different from that of the **1** versus $NaBH_4$, (Figure IV-24) e.g. the λ_{max} value undergoes a change from 355 nm to 257 nm in **1**.

(2) The $NaBH_4$ reduction product (**1R**) from **1** has been isolated and characterized to be a Ni(I) – 7, 8,- dihydropterin complex. It is a dark colored moisture sensitive product. The color changes associated with $NaBH_4$ reduction (yellow-green → dark color) is shown in Figure IV – 26.

(3) In chapter II it has been pointed out that the Cu(II)-pterin-phen mixed ligand complex, on $NaBH_4$ reduction provides with a Cu(I) complex, where the pterin ligand is in the 7,8-dihydro state.

It is worthwhile to explore the ability of **1R** to activate dioxygen for hydroxylation purpose towards a typical aromatic substrate like bromobenzene.[55] Next section describes such an endeavor for modeling the PAH type activity.[7,8,52-55]

(4) Last but not the least **1** is the only member of the present series of examples discussed here [e.g. the corresponding Cu(II) and Co(II) – systems have been presented in chapters II and III respectively] which is able to exibit substrate saturation kinetics with respect to both group transfer [Figure IV-23] and redox reagents [Figure IV-25] respectively.

Reactivity of 1R with bromobenzene and dioxygen.

Figure IV-27 shows the absorption spectral changes during reaction of **1R** (obtained by $NaBH_4$ reduction of **1**) with bromobenzene in CH_3OH medium saturated with dioxygen. Hardly any isosbestic point could be observed in the relevant spectral change behavior, which can be taken as an indication for the presence of an intermediate step, during conversion of the substrate (bromobenzene) to the product. A closer scrutiny of Figure IV-27(a) indicates that the initial fast step (upto ca. 200s), in followed by a brief pause (ca. 200 – 300 s region) and then the gradual conversion to the final product continues (beyond 1000 s). Kinetics of this reaction was followed at 365 nm and four different temparatures (range: 300 – 330K) in CH_3OH saturated with O_2 under psudo-first-order conditions (using a **1R** : bromobenzeneratio of 1 : 140); the entropy of

activation parameter ($\Delta S^{\neq}$) was evaluated from the Eyring plot. The relevant data are indicated below:

k_{obs} = 1.4 x 10^{-2} s^{-1} ; $\Delta S^{\neq}$ = - 191.6 J $mol^{-1}deg^{-1}$.

The negative $\Delta S^{\neq}$ value indicates an associative pathway, while the k_{obs} value is consistent with a group transfer process.[92] As suggested from DFT studies on the mechanistic pathway of PAH activity using the x-ray structural data of a PAH enzyme,[99] formation of an initial dioxygen – **1R** complex is quite likely whereby the dioxygen entity is activated through Ni(I)→O_2 electron transfer, leading to subsequent hydroxylation of bromobenzene.

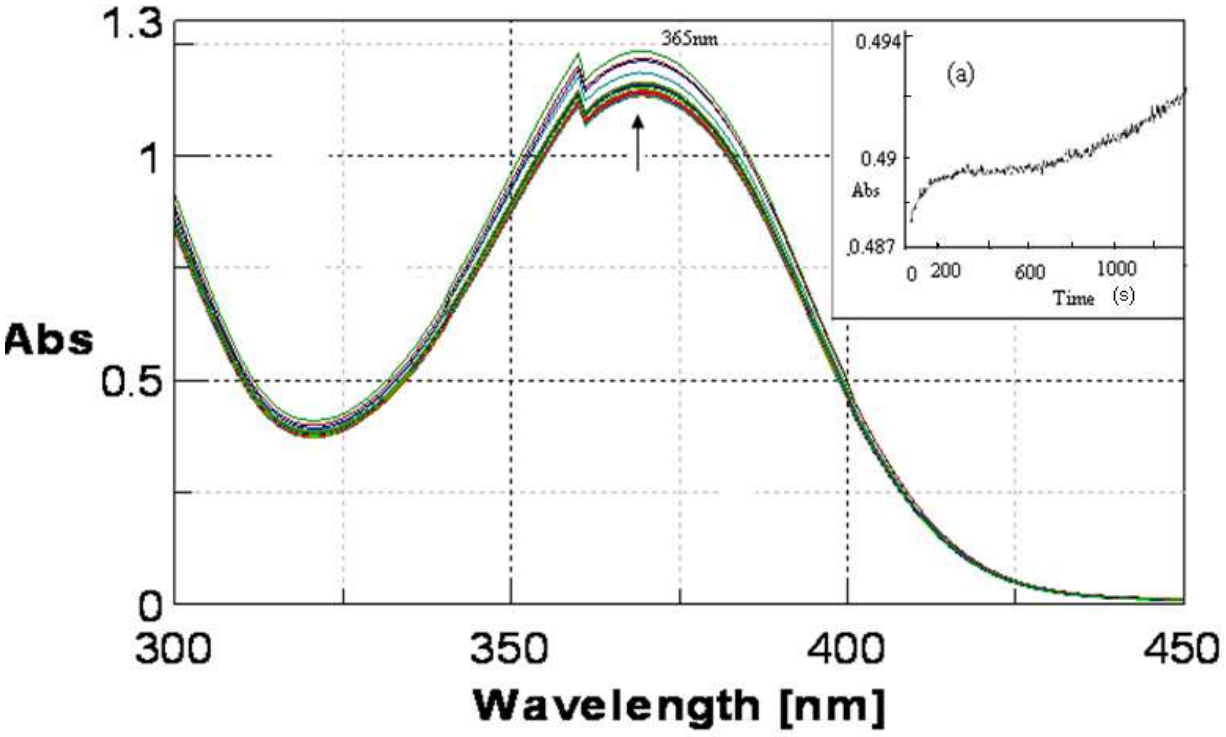

Figure IV-27. Absorption spectral changes recorded at 1.5 min interval during the reaction of **1R** (5.8x10^{-5}M) with bromobenzene (4.59x10^{-3}M) in CH_3OH, saturated with O_2 (a)Absorption spectral changes recorded at 365 nm represent the absorbance versus time curve at 311K.

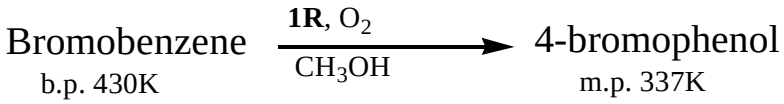

Stoichiometry of this reaction was established by repeating it on the preparative scale and recovering 4-bromophenol as a white solid (m.p.337K) from the reaction medium. Here the initial step is concerned with the formation of O_2 – **1R** intermediate complex, activation of the O_2 moiety through transfer of reducing equivalents from the Ni(I) centre/ 7, 8-dihydro pterin ring of **1R** and the release of an electrophilic oxygen atom. The latter completes the formal hydroxylation step.

1st step

2nd step

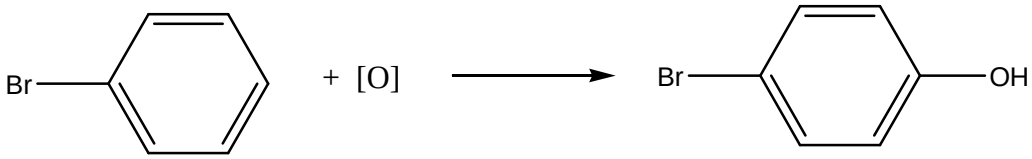

The most crucial step is the activation of the dioxygen entity.

Further light is thrown on the above mechanistic pathway by **2** and its $NaBH_4$ reduction product **2R,** as presented below.

Reactivity of 2 towards $NaBH_4$

Figure IV-28 shows the reaction profile for the interaction of **2** with $NaBH_4$ in CH_3OH. Unlike for the corresponding reaction between **1** and $NaBH_4$ (Figure IV-24), we find the appearance of two isosbestic points at 265 nm and 400 nm respectively; close approach to such a behavior is observed at 345 nm. This drastic change over in reactivity behavior towards $NaBH_4$ could be achieved simply by substituting the aquo group of **1** by an imidazole (Im) group in **2**. [Figure IV-1 and IV-2]. Table IV-6 shows the effect of imidazole substitution on the relevant

geometric parameters together with the Δ(= **1** – **2**) values (Å). Although the magnitudes of most of the Δ values are small, few of them are sufficient to affect the reactivity behavior. Table IV-8 shows few classic parameters on the electron transfer rate constants.[79] A change over in size by around 0.04 – 0.09 Å could affect the rate constants by an order of 10^3 – 10^5. This is essentially the Franck-Condon barrier to electron transfer reactions.[79] Besides this, the reactivity behavior of **1** towards $NaBH_4$ conforms to substrate saturation kinetics [Figure IV – 25] which presupposes the formation of an intermediate like [**(1)**$NaBH_4$] (Scheme IV-13). But for **2**, the Figure IV -28 indicates an almost clean conversion **2→2R**. Most likely the absence of an aquo group in **2** prevents the formation of an intermediate complex with $NaBH_4$, as indicated above for **1**. The relevant kinetic parameters are shown below.

k_{obs} = 9.0 x 10^{-3} s^{-1}; $\Delta S^{\neq}$ = - 186.0 J K^{-1} mol^{-1}.

The negative $\Delta S^{\neq}$ value is consistant with an associative pathway involving both group (hydride ion) and electron transfer process. This k_{obs} value is quite close for that of the reaction between **1** and $NaBH_4$ (Figure IV-24; k_{obs} = 8.8 x 10^{-3} s^{-1}), but the reaction pathway is different, as indicated above.

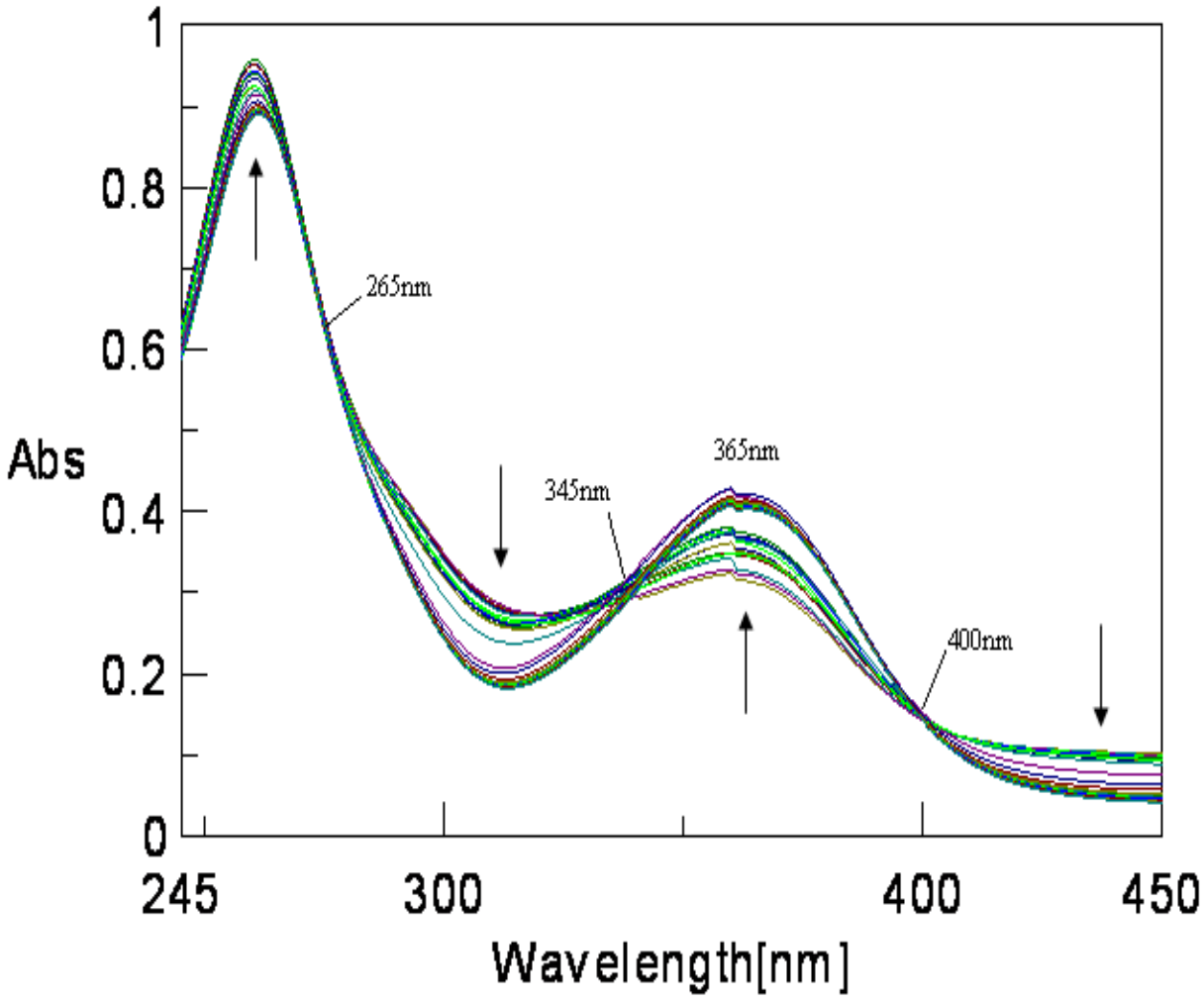

Figure IV-28. Absorption spectral changes recorded at 1.5 min interval during the reaction of (**2**) ($5.8x10^{-5}$M) with $NaBH_4$ ($4.59x10^{-3}$M) in CH_3OH at 311K

Table IV-8. Some outer-sphere electron-exchange reaction.

Reacting pair	Electron configuration	Rate ($L\ mol^{-1}\ s^{-1}$ at 25°C)	Difference in M—L bond lengths (Å)
$[Fe(bipy)_3]^{2+/3+}$	t_{2g}^6/t_{2g}^5		0.00 ± 0.01
$[Mn(CN)_6]^{4-/3-}$	t_{2g}^5/t_{2g}^4		
$[Mo(CN)_8]^{4-/3-}$	[a]	>10^6	Very small
$[W(CN)_8]^{4-/3-}$	[a]		
$[IrCl_6]^{3-/2-}$	t_{2g}^6/t_{2g}^5		
$[Os(bipy)]^{2+/3+}$	t_{2g}^6/t_{2g}^5		
$[Fe(CN)_6]^{4-/3-}$	t_{2g}^6/t_{2g}^5	~10^5	
$[Ru(en)_3]^{2+/3+}$	t_{2g}^6/t_{2g}^5	4 × 10^4	
$[Ru(NH_3)_6]^{2+/3+}$	t_{2g}^6/t_{2g}^5	4 × 10^3	0.04 ± 0.01[b]
$[Ru(H_2O)_6]^{2+/3+}$	t_{2g}^6/t_{2g}^5	20[c]	0.09 ± 0.02[b]
$[Fe(H_2O)_6]^{2+/3+}$	$t_{2g}^4e_g^2/t_{2g}^3e_g^2$	4	0.14 ± 0.02[b]
$[MnO_4]^{2-/1-}$	[a]	>10^3	
$[Coen_3]^{2+/3+}$			
$[Co(NH_3)_6]^{2+/3+}$	$t_{2g}^3e_g^2/t_{2g}^6$	~10^{-4}	0.18 ± 0.02
$[Co(C_2O_4)_3]^{4-/3-}$			

Ref. 79, F.A. Cotton and G. Wilkinson, Advanced Inorganic Chemistry, 5th ed (1988). p1308. John Wiely & Sons, New York.

Reactivity of 2R with bromobenzene/ O_2 reaction mixture

Reactivity of **2R** with bromobenzene in presence of dioxygen was studied and the relevant reaction profile is shown in Figure IV-29. Two isosbestic points at 265 nm and 400 nm respectively, characterized this reaction process, whereas reaction stoichiometric study afforded the isolation of 4-bromophenol from the reaction medium. Almost a clean conversion to the hydroxylated product is indicated. This reaction profile is completely different from that of **1R**

with bromobenzene/O_2 mixture [Figure IV-27]. Once again the imidazole substitution at the metal centre could achived this change over in kinetic behavior (Tables IV-6 and IV-8). The following kinetic data are obtained for the above process [Figure IV-29]:

$k_{obs} = 8.8 \times 10^{-3}\ s^{-1}$; $\Delta S^{\neq} = -178.0\ J\ K^{-1}\ mol^{-1}$.

Once again, an associative pathway is indicated, for the following process, which takes place in

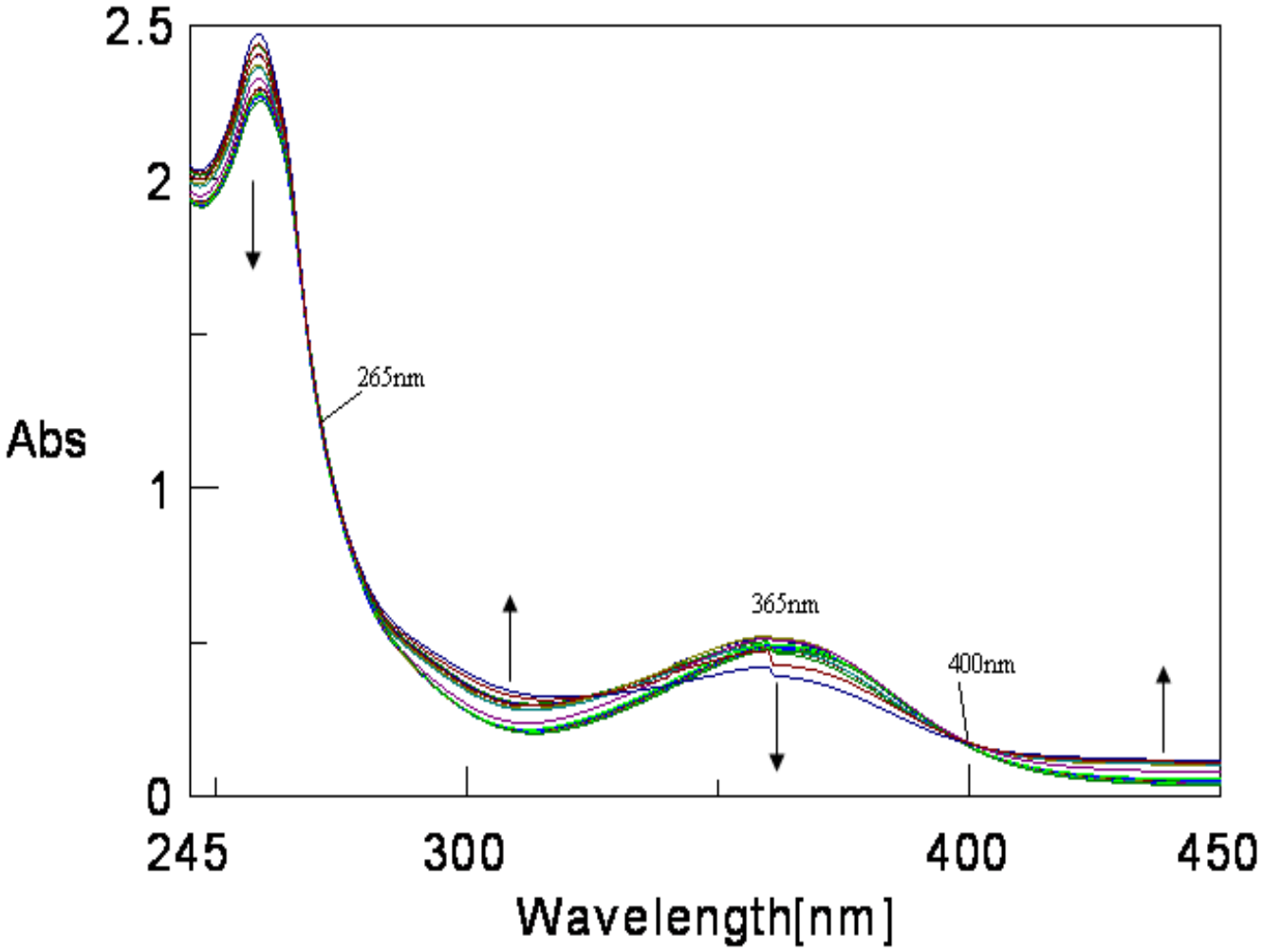

Figure IV-29. Absorption spectral changes recorded at 1 min interval during the reaction of (**2R**) (5.8×10^{-5}M) with bromobenzene (4.59×10^{-3}M) in CH_3OH saturated with dioxygen (O_2) at 311K.

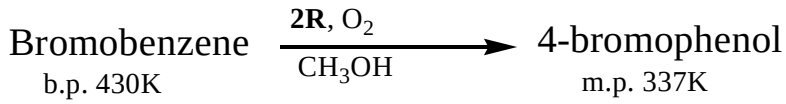

essentially one step.

Now a comparison of Figure IV-28 and IV-29, together with the corresponding k_{obs} values of 9.0×10^{-3} s^{-1} and 8.8×10^{-3} s^{-1} respectively, indicates that the transfer of reducing equivalents (from $NaBH_4$) to **2** and the onwards transformation of the same (from **2R**) to the bromobenzene/O_2 reaction mixture, take place in one step in either case, at almost same rate.

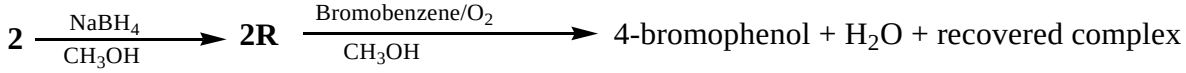

Only difference between the above two spectra is the movement of the arrows indicating the spectral change behavior; even the positions of the isosbestic points remain unchanged. The above reactivity steps highlight the ability of the present nickel (II)-pterin complexes to assimilate reducing equivalents from $NaBH_4$ and further to activate the aromatic ring of bromobenzene towards hydroxylation; in other words, they may be treated as functional models of phenylalanine hydroxylase (PAH).[7,52-55,99-101]

The most interesting aspect of this study is that fine tuning of the metal centre through substitution of an imidazole group could achieve an enormous change over in kinetic behavior from a substrate saturation process to another involving essentially one step conversion.

Reactivity of 2R with $K_3[Fe(CN)_6]$

The relevant reaction profile is shown in Figure IV-30 indicating an almost clean oxidation reaction with isosbestic points at 265 nm and 400 nm respectively. Apart from the positions of the isosbestic points, the directions of movement of the spectral curves are quite similar to that in Figure IV- 29. In either case the reaction profile highlights the transfer of reducing equivalent away from **2R,** as mentioned earlier such reducing equivalents were transferred to **2** [**2**+ $NaBH_4$ → **2R**] by $NaBH_4$ (Figure IV-28). The spectral change behavior is quite well-defined for the reaction with $K_3[Fe(CN)_6]$ (Figure IV-30). Kinetics of the reaction was followed at 360 nm under psudo-first-order condition [using a **2R** : $K_3[Fe(CN)_6]$ ratio of 1: 100] and four different temperatures (300 – 330K) in CH_3OH-H_2O (3: 1 v/v).

The following kinetic parameters were evaluated:

$k_{obs} = 3.6 \times 10^{-2}\ s^{-1}$; $\Delta S^{\ddagger} = -184.0\ J\ K^{-1}\ mol^{-1}$.

A comparison of the k_{obs} data with that of **2R** with bromobenzene/O_2 mixture, indicates an almost 4 times increase in reaction rate with $K_3[Fe(CN)_6]$.

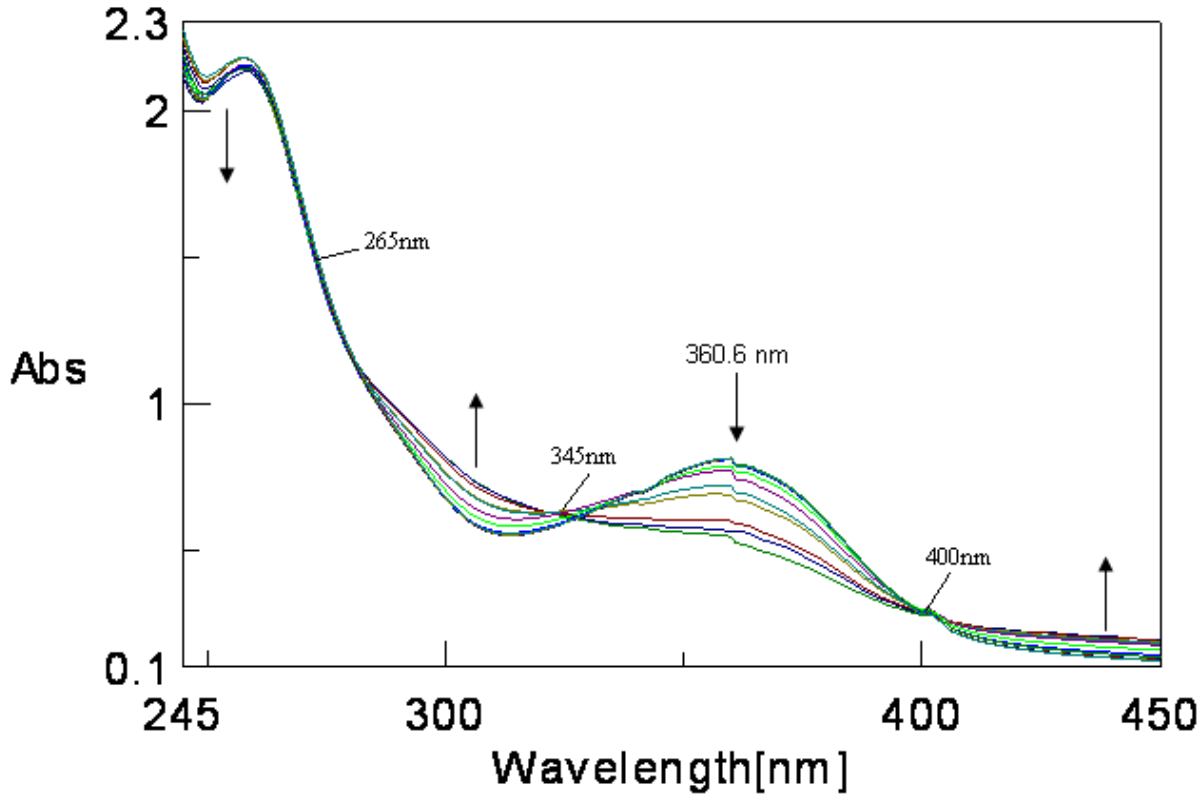

Figure IV-30. Absorption spectral changes recorded at 15 second interval during the reaction of (**2R**) (5.8×10^{-5}M) with $K_3[Fe(CN)_6]$ (4.59×10^{-3}M) in CH_3OH - H_2O (3:1 v/v) at 298K.

Figure IV -31 shows an attempt for exploring reactivity between $NaBH_4$ and $K_3[Fe(CN)_6$ in CH_3OH –H_2O (3:1 v/v) medium at 320K. Hardly any reactivity is observed in this case, indicating no direct transfer of reducing equivalents from $NaBH_4$ towards $K_3[Fe(CN)_6]$. As evident from the above discussion, this Ni(II)-pterin complex serves as an excellent mediator for

transferring reducing equivalents from $NaBH_4$ to either a model substrate like bromobenzene in presence of O_2 or a biochemically relevant oxidizing agent like $K_3[Fe(CN)_6]$ [E° = 0.36 V]. It may be stated in this conection that NAD^+ and $NADPH^+$ can be reduced nonenzymatically by reducing agents like sodium dithionite or sodium borohydride. NADH and NADPH can in turn be nonenzymatically reoxidized with ferrecyanide, but they are not oxidized directly by molecular oxygen at pH 7.4.[94] Activation of dioxygen through Ni(I)→O_2 electron transfer, is most possibly responsible for above ability of **2R**, which in turn is obtained through the $NaBH_4$reduction of **2**.[99] It has already been pointed out that **2R** is a Ni(I)-7,8-dihydro pterin complex. The dihydro pterin ring could supply the reducing equivalents needed to reduce one of oxygen atoms of O_2 to the level of H_2O and releasing the other oxygen atom required for the conversion bromobenzene → 4-bromophenol

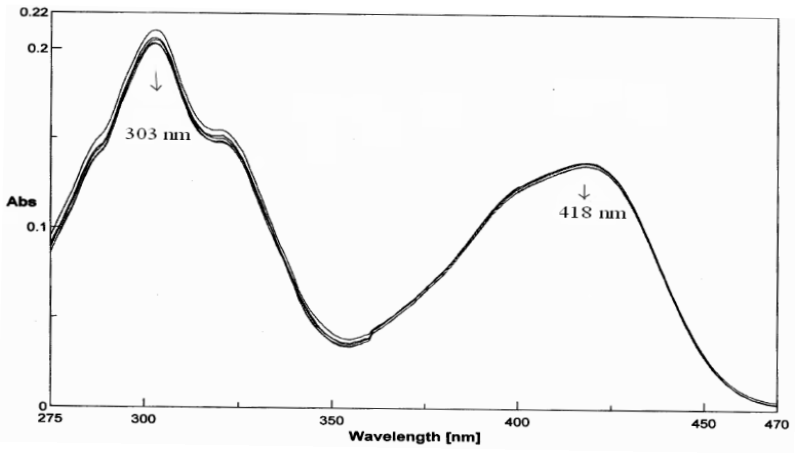

Figure IV- 31. Absorption spectral data recorded at 10 min interval for exploring the reactivity between $NaBH_4$ ($1.2x10^{-4}$ M) and $K_3[Fe(CN)_6]$ ($1.2x10^{-4}$M) in CH_3OH-H_2O (3:1 v/v) at 320 K.

In other words, dioxygen is activated here for performing the tusk of hydroxylating an aromatic ring. The above conversions can be summarized in terms of the following scheme:

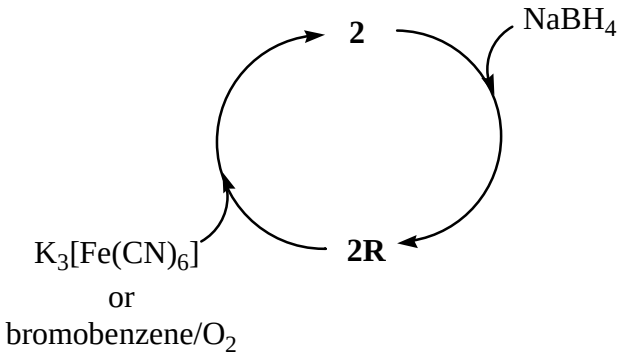

Scheme IV-14

In terms of Figures IV-28 – IV-30, the above transfer of two reducing equivalents [O_2 + [2H] → H_2O + incipient oxygen atom (O)] takes place simultaneously.[94]

Electronic structures of 1 and 2 : Correlation with reactivity

DFT calculations were performed with the Gaussian 09 package using the B3LYP hybrid functional and the 6-31g basis set.[95,96] Starting parameters for complex **1** and **2** were taken from their refined crystal structure parameters.[17c,d] Geometry optimization was not carried out separately as here the structures were obtained from the refined crystal parameters. The ground state energy minimization was carried out and the energy level diagrams of the selected frontier molecular orbitals were obtained (figure IV-32). This diagram also indicates information about the compositions of the relevant frontier orbials. Few relevant band gaps (eV) are also indicated in Figure IV-32. For several cases the energy band gap between adjacent levels is quite low (0.11 – 0.3 eV). In recent years synthetic molecules with exceptionally small (< 0.5 eV) band gaps are receiving considerable attention due to their interesting electrochemical/redox amphoteric behavior.[64,66] Usually in such cases the HOMO – LUMO orbitals are located in different

covalently linked centers within the same molecule. Thermo-excited intarmolecular electron transfer can

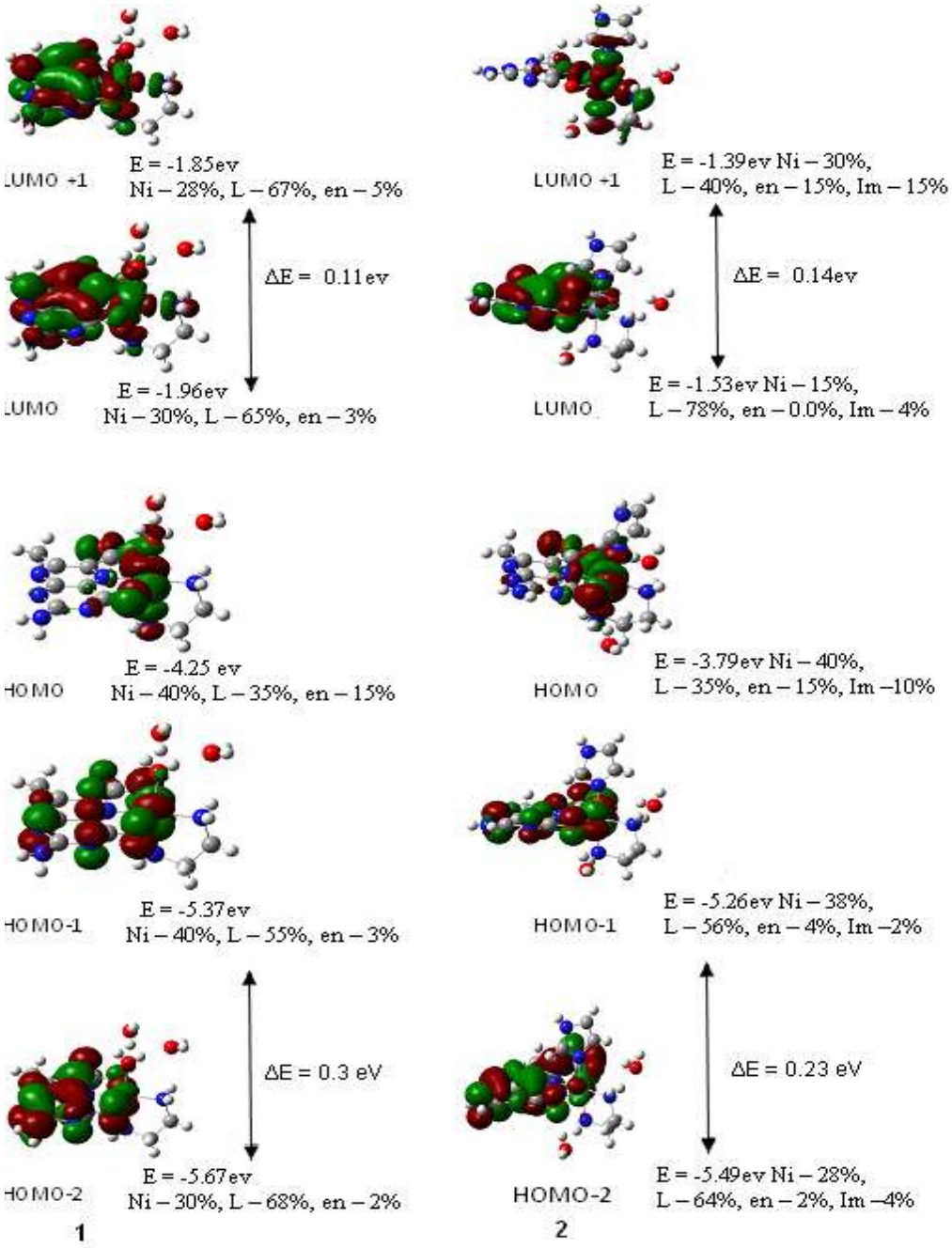

Figure IV-32. Frontier molecular orbitals of **1** and **2**, showing their energies (eV) and compositions (%).

take place between two such centers in solution. The combination of the redox non-innocent pterin ligand residue with the redox active metal centre [Ni(II) → Ni(I)] in complexes **1** and **2,** leads to such a situation here, associated with distinct redox activities.[9-11,53] For **2** additional stereoelectronic factor comes into play due to the presence of π-acidic imidazole ligand, with a definite contribution (10-15%) to the HOMO and LUMO +1 levels respectively. For both **1**and **2** the HOMO-1 and HOMO-2 levels are characterized small band gaps (0.23 – 0.3 eV). Such gaps are still smaller (0.11 – 0.14 eV) for the corresponding LUMO and LUMO+1 levels. The latter aspect may be taken as reason for the facile reaction of **1** and **2** with $NaBH_4$, leading to the transfer of reducing equivalents to the aforesaid vacant energy levels. Now a closer look may be taken at the compositions of the frontier orbitals. For example, in case of **1** the pterin (65-67%) and Ni(II) centrs (28-30%) make major contributions to the LUMO and LUOM+1 levels. For **2** the LUMO+1 level is composed of almost equal shares of Ni(II), pterin and the ancillary ligands. That is, there is a substantial lowering of contribution to the LUMO+1 level from pterin in case of **2**. This aspect may be as one of the reasons for the different reactions profiles of **1** and **2** (Figure IV-24 & IV-28; IV-27 & IV-29). Besides this, the steric factors as par Tables IV-6 and IV-8, may be partly responsible for the above reactivity differences.

Now a closer look may be taken at the cyclic voltammetry data of **1** and **2** (Figure IV-19 – IV-21**)** in the light of Figure IV-32 as well as Scheme IV -11, showing the Frost diagram of the Ni(II) – Ni(I) centres. For both **1** and **2** there is a small band gap between the LUMO and LUMO +1 levels, indicating the easy reduction of the Ni(II) centre. Besides this, the small energy change over (Scheme IV-11), associated with Ni(II) →Ni(I) transformation, may be responsible for the appearance of the above metal-centered reduction peak in cyclic voltammetry. The Ni(I) species has a lower life time in aqueous medium(Figure IV-20).

Conclusion

This chapter is concerned with detailed studies on two new nickel(II)-pterin complexes.They could be synthesized and crystallized out of the aqueous medium, a reasonable synthetic achievement, as non aqueous medium is usually needed for such synthesis. These x-ray structurally characterized complexes, permit the recording of a wide variety of physico-chemical and reactivity data and their meaningful interpretation. The ESIMS, IR, UV-VIS data are consistent with their chemical compositions. Their CD spectral data throw light on the conformation of the chelate ring of the ancillary ligand "en". Hence the positive cotton effect around 755-769 nm, is correlated with the δ-conformation of "en" ring. $NaBH_4$ reduction of both these complexes could be achived and such reductions are associated with a substantial increase in fluorescence emission intensity, indicating increase in electron density in the resulting reduced complexes. Cyclic voltammetric data of **1** and **2** indicate the formation of the corresponding Ni(I) species on the time scale of cyclic voltammetry; this reduced species has a longer life time in DMSO as compared to that in the aqueous medium. Reactivity of **1** with both imidazole and $NaBH_4$, follow substrate saturation kinetic path way. No other compound of this treatise possess this attribute. The $NaBH_4$ reduced complex **1R** (Figure IV-26) could be isolated in the solid state and characterized to be a Ni(I) complex of the 7,8-dihydro form of the pterin ligand.[22,23] In other words, reducing equivalents are transferred to both the metal and pterin ligand centers of **1** → **1R**. Reactivity of **1R** towards a reaction mixture of bromobenzene/O_2 could be followed both kinetically and stoichiometrically. Here bromobenzene has been utilized as a model substrate for following the phenylalanine hydoxylase (PAH) type activity of **1R**; isolation of 4-bromophenol from the reaction medium reveals the ability of **1** to act as a functional model here in transferring reducing equivalents from $NaBH_4$ to the bromobenzene/O_2 reaction mixture through the **1R**

stage. Most likely, a Ni(I)→ O_2 electron transfer initiates the process of dioxygen activation, followed by hydroxylation of the aromatic ring of bromobenzene.

From consideration of kinetic application of crystal field theory to the substitution process of octahedral complexes involving the associative pathway, it appears that the crystal field contribution to the total activation energy (E_{CFAE}), makes definite contribution to d^3, spin paired d^6 and d^8 systems, predicting slower reaction rates.[97,98] In any mechanism the most important single factor is the strength of the bond between the central atom and the leaving group. Only a small part of this bond energy is related to crystal field effects. Changes in metal-ligand attractions, ligand-ligand repulsion, etc., make large contribution to the activation energy. For **1** the positive E_{CFAE} value and the presence of the aquo group make it suitable for substrate saturation kinetics (Figure IV-22 to IV-25 as well as IV-27). Literature data for Ni(II) complexes indicate lability for a σ-donor ligand like H_2O/en, but inertness for a π-acceptor ligand like phen/bipy.[63] In **2** an imidazole group (π-acceptor type ligand) replaces the aquo group and could achieve a complete change over in kinetic behavior (Figure IV-28 and IV-29) to one-step process. Even the oxidation of **2R** by an essentially transfer agent like $K_3[Fe(CN)_6]$ (Figure IV-30) is an one-step process, with the change over point at 345 nm (LMCT region) being more clearly defined. On the other hand, for reactions with group transfer agent like $NaBH_4$ or bromobenzene/O_2 mixture (Figure IV-29), the LMCT region (≈ 345 nm) is quite spread out, indicating the participation of at least a couple of species differing in their oxidation state of the pterin ring (7, 8- dihydro state → oxidized/aromatic state) as well as Ni(I)-pterin → Ni(II)-pterin bonding change over. The frontier orbital energy level diagram (Figure IV-32) is helpful for rationalizing some of the unique redox activity aspects, in terms of small energy band gaps as well as composition of such energy levels. The Frost diagram (SchemeIV-11) is able to justify

the isolation of the Ni(I) – 7, 8-dihydropterin complexes (**1R,2R**) in the solid state. On the basis of the above deliberations, it is reasonable to consider **1** and **2** as functional models for PAH-type activity with bromobenzene as the model substrate and $NaBH_4$ as a model of NADH/NADPH in transferring reducing equivalents to the model active sites of **1** and **2**, needed for the following purpose:[22,23,53]

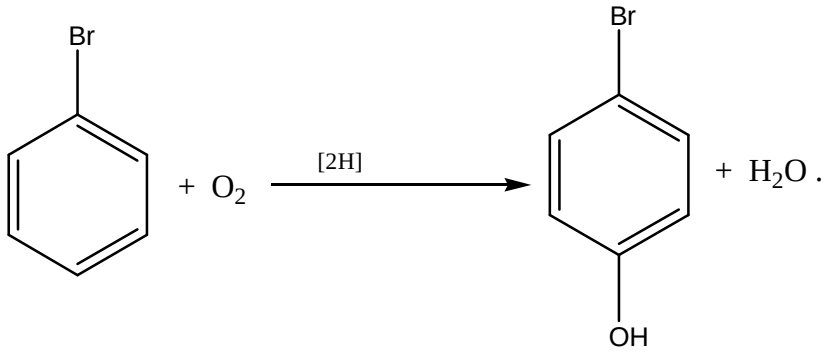

Most likely, the Ni(I)→O_2 electron transfer step initiates the process of dioxygen activation, with the 7, 8 – dihydro form of the pterin ring. (of **1R, 2R**) completing the process of reducing equivalent, [2H] transfer. For **1R,** it is a two- step process (Figure IV-27), while **2R** completes this process in essentially a single step (Figure I-29).